Enhancing gene co-expression network inference for the malaria parasite *Plasmodium falciparum*

Qi Li[1,3,4], Katrina A Button-Simons[2,4], Mackenzie AC Sievert[2,4], Elias Chahoud[1,5], Gabriel F Foster[2], Kaitlynn Meis[2], Michael T Ferdig[2,4], and Tijana Milenković[1,3,4,*]

1 Department of Computer Science and Engineering; 2 Department of Biological Sciences; 3 Eck Institute for Global Health; 4 Lucy Family Institute for Data & Society; 5 Department of Preprofessional Studies, University of Notre Dame, Notre Dame, IN, 46556, USA.

*** tmilenko@nd.edu**

Abstract

Background: Malaria results in more than 550,000 deaths each year due to drug resistance in the most lethal *Plasmodium* (*P*) species *P. falciparum*. A full *P. falciparum* genome was published in 2002, yet 44.6% of its genes have unknown functions. Improving functional annotation of genes is important for identifying drug targets and understanding the evolution of drug resistance. **Results:** Genes function by interacting with one another. So, analyzing gene co-expression networks can enhance functional annotations and prioritize genes for wet lab validation. Earlier efforts to build gene co-expression networks in *P. falciparum* have been limited to a single network inference method or gaining biological understanding for only a single gene and its interacting partners. Here, we explore multiple inference methods and aim to systematically predict functional annotations for all *P. falciparum* genes. We evaluate each inferred network based on how well it predicts existing gene-Gene Ontology (GO) term annotations using network clustering and leave-one-out cross-validation. We assess overlaps of the different networks' edges (gene co-expression relationships) as well as predicted functional knowledge. The networks' edges are overall complementary: 47%-85% of all edges are unique to each network. In terms of accuracy of predicting gene functional annotations, all networks yield relatively high precision (as high as 87% for the network inferred using mutual information), but the highest recall reached is below 15%. All networks having low recall means that none of them capture a large amount of all existing gene-GO term annotations. In fact, their annotation predictions are highly complementary, with the largest pairwise overlap of only 27%. We provide ranked lists of inferred gene-gene interactions and predicted gene-GO term annotations for future use and wet lab validation by the malaria community. **Conclusions:** The different networks seem to capture different aspects of the *P. falciparum* biology in terms of both inferred interactions and predicted gene functional annotations. Thus, relying on a single network inference method should be avoided when possible. **Availability and implementation**: All data and code are available at `https://nd.edu/~cone/pfalGCEN/`.

Introduction

Motivation and related work

Malaria is a deadly disease caused by protozoan parasites of the genus *Plasmodium* (*P.*) that are transmitted by the bite of female mosquitoes [50, 65, 67]. The most deadly malaria species *P. falciparum* causes more than 0.5 million deaths annually, mostly among children under five years

old [16, 51, 52, 77]. Sub-Saharan Africa accounts for 79.4% of malaria cases and 87.6% of deaths [51, 74]. *P. falciparum* has evolved resistance to all antimalarial drugs, making treatment difficult in areas where multidrug resistant parasites are common [13, 26, 30, 36, 42]. The *P. falciparum* research community has developed tools to quickly identify mutations that can be used as markers for drug resistance and genes that are under selection. For some drugs a causal gene has been identified that is the main driver of drug resistance [25]. However, understanding how mutations in that gene confer resistance is a more difficult problem to solve. Unfortunately, 44.6% of genes in the *P. falciparum* genome have unknown function. This lack of knowledge of gene function represents a key challenge to a better understanding of how mutations confer drug resistance. In particular, Gene Ontology (GO) annotations that are often used to describe the biology (e.g., biological processes, molecular-level activities, or cellular structures and localization) of genes are deficient for *P. falciparum* [49]. Deriving novel gene-GO term associations would be a valuable contribution to *P. falciparum* gene annotations.

Because biological functions that lead to key traits like drug resistance are controlled by many interacting genes, studying them as complex networks of gene-gene (or protein-protein) interactions presents promising analytical approaches to uncovering important *P. falciparum* biology [23]. Despite pioneering efforts to obtain physical protein-protein interaction (PPI) data for *P. falciparum* [18, 34], high-quality data of this type are lacking [55]. This increases the urgency to understand other interaction/network types. Fortunately, a wealth of gene expression data is available for *P. falciparum* [21], from which gene co-expression networks can be constructed. Gene co-expression networks can be powerfully applied because genes that are functionally related (i.e., that are annotated by the same GO terms) are likely to be co-expressed [73]. Consequently, analyses of a gene co-expression network, where nodes are genes and edges are co-expression relationships between genes over different conditions (e.g., time points or drug treatments), is a valuable tool for identifying novel (i.e., currently unknown) gene-GO term annotations.

Earlier efforts to build gene co-expression networks in *P. falciparum* have been limited to a single network inference method such as mutual information (MI) [60] or absolute value of the Pearson Correlation Coefficient (absPCC) [6, 64], leaving other potentially powerful gene co-expression network inference approaches unexplored. Prominent examples include a tree-based measure called Random Forest (RF) [24] and Adaptive Lasso (AdaL) [32]. In fact, it was shown in different species (baker's yeast, brewer's yeast, *E. coli* and *Staphylococcus aureus*) that networks resulting from different gene co-expression network inference methods may be able to give insights into different biological questions [56] and capture different types of regulatory interactions [43]. In addition to investigating *P. falciparum* biology utilizing a single network inference method to build gene co-expression networks, previous efforts have asked limited biological questions about the interacting partners or functions of particular genes [1, 21, 60, 66, 79]. However, gene co-expression networks developed using multiple inference methods have not yet been developed for *P. falciparum*. It is unknown whether different network inference methods capture different aspects of *P. falciparum* biology and whether they could inform the important task of systematically predicting GO term annotations for all *P. falciparum* genes.

Here, we fill this gap by constructing multiple co-expression networks using four prominent network inference methods (MI, absPCC, RF, and AdaL) and evaluate them for systematic, comprehensive, and accurate predictions of gene-GO term associations. Furthermore, we assess the extent to which the networks are complementary or redundant in terms of their edges (i.e., gene co-expression relationships) as well as predicted functional knowledge. Finally, we apply our inferred networks to the study of endocytosis, an essential biological process involved in *P. falciparum* drug resistance.

Our study and contributions

We analyze gene expression data consisting of 247 samples corresponding to 247 combinations of drug treatments and time points [21] (Fig. 1). We apply four network inference methods to this expression data to infer their respective co-expression networks. Each network inference method mathematically assigns a weight representing the strength of a co-expression relationship between a pair of genes. The highest-weighted gene (i.e., node) pairs are kept as edges in the given network. To choose a weight threshold for distinguishing between edges and non-edges in a network, we adopt a prominent network inference framework called ARACNe [44].

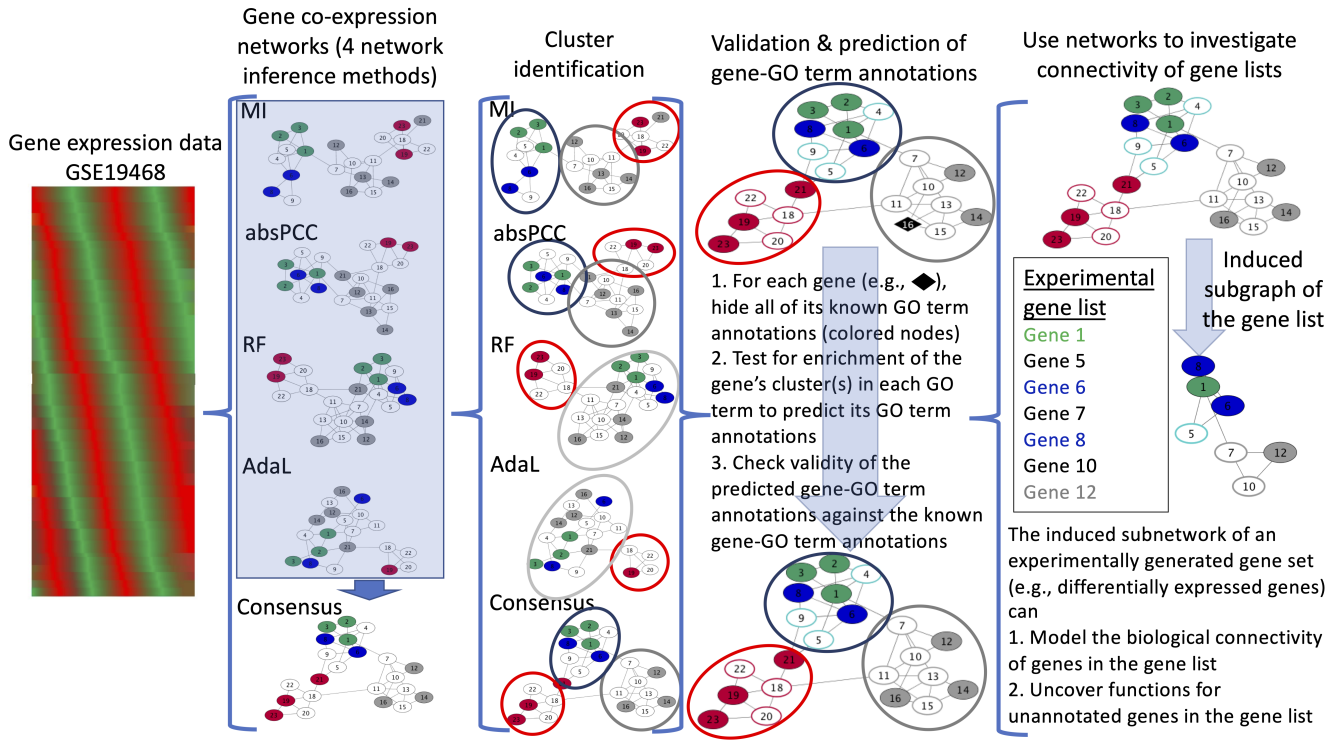

Figure 1. Summary of our generalizable framework for gene co-expression network construction, validation, and biological application. We use four network inference methods MI, absPCC, RF, and AdaL) to construct gene co-expression networks of *P. falciparum*. We also generate a Consensus network by combining the four individual networks. We use two clustering methods to identify gene clusters (functional modules) in each network. Then, we use cross-validation to examine how well each network's clusters correspond to known GO terms. In other words, GO term annotations are comprehensively predicted for all genes whose clusters are statistically significantly enriched in at least one GO term, and the predicted gene-GO term annotations are then contrasted against the known ones. The Consensus network is used to investigate connectivity of genes in a list or a gene set; in our biological application, we investigate lists of genes that interact with three proteins involved with the biological process of endocytosis.

We find that the co-expression networks resulting from the different inference methods are overall highly complementary (i.e., non-redundant). Namely, the networks constructed using MI, absPCC, and AdaL, share only 15%-53% of the edges; that is, 47%-85% of the edges are unique to each of the networks. Only the network resulting from RF is mostly redundant to the networks resulting from the other three inference methods. This indicates that the different network inference methods largely capture unique features of gene co-expression relationships. Given so many unique edges in almost all networks, we consider an additional co-expression network that integrates (takes union of) the edges from all of the individual networks; we refer

to this network as Consensus.

Consequently, we use gene-GO term annotations (or associations) to assess each co-expression network by leveraging data from GeneDB [1] and PlasmoDB [2] databases. We generate predictions by hiding a portion of the existing gene-GO term annotations (or associations) and evaluating how well they are recovered from a given network using cross-validation. Specifically, we use a common paradigm for predicting function annotations called network clustering. A cluster is a group of genes in a network that are densely connected to each other or have similar topological patterns. A cluster is deemed functionally meaningful if a statistically significantly high number of genes are annotated by the same GO term. By extension, we can then predict the other genes in this cluster to also be annotated by this GO term. We compare the predicted annotations with the hidden portion of the existing gene-GO term annotations to evaluate the accuracy of a given network. We test two clustering methods (i.e., cluster affiliation model for big networks – BigCLAM, referred to as BC [78], and Markov Clustering – referred to as MCL [14]) as well as multiple parameters for each clustering method. We use these clustering methods because they are highly prominent [15, 40, 41, 47, 53, 72], and also, MCL has been shown to perform consistently well [11, 40, 47, 71, 72].

We evaluate networks based on their prediction accuracy scores, i.e., precision and recall. Precision measures the fraction of predicted annotations that are correct (i.e., currently known); recall measures the fraction of all known annotations that are predicted. Generally there is a trade-off between precision and recall: higher precision typically means lower recall, and vice versa. In biomedical applications, precision is typically favored over recall [31, 35, 38, 39, 48] because confirmatory lab experiments are time consuming and expensive and it is often preferred to follow-up on a few higher-quality predictions than many lower-quality ones. In our own analysis, while some of the networks generate precision scores as high as 87%, the highest recall reached is below 15%. The MI method generates the highest precision and the others also have reasonably high precision scores. All networks have relatively low recall indicating that none capture a large amount of all existing gene-GO term annotations. In fact, we find the different networks' predictions to be highly complementary to each other (i.e., the maximum prediction overlap over all network pairs is only 27%). Hence, the different networks seem to capture different aspects of the *P. falciparum* biology, as was the case in baker's yeast [56].

To supplement the limited functional annotation data in the *P. falciparum* genome, we assign a confidence score to each (known and novel) predicted gene-GO term association based on how many networks support the given prediction. Similarly, we assign confidence scores to the inferred gene-gene interactions. We provide the confidence score-ranked lists of functional predictions and interactions for future community use that could be especially useful given the paucity of comprehensive functional annotations as well as high confidence PPI data for *P. falciparum*.

In addition to validating inferred networks via gene functional prediction, we investigate the connectivity of genes hypothesized to function together in a biological process. That is, we apply our network approach to recently generated lists of endocytosis-related genes in *P. falciparum* [7]. Endocytosis is an essential biological process for trafficking extracellular material to specific organelles in the cell. Extracellular material is first brought into the cell by early endosomes that mature into late endosomes as they are directed to lysosomes or through the trafficking pathways from the Golgi apparatus. The *P. falciparum* proteins Kelch13 and EPS15 have been localized to the periphery of the cell and suggested to participate in the machinery to generate early endosomes. The *P. falciparum* protein clathrin functions in an atypical role, primarily through trafficking pathways of the Golgi apparatus in other apicomplexan organisms with similar functions suggested in *Plasmodium* [20, 54]. Kelch13 (K13) is a molecular determinant of artemisinin resistance. EPS15 is a close interacting partner of K13 and typically functions in canonical endocytosis pathways [68], and clathrin is also the main structural protein

[1] `https://www.genedb.org/`
[2] `https://plasmodb.org/plasmo/app`

in clathrin-dependent endocytosis. Recently, Birnbaum *et al.* [7] experimentally determined protein-protein interaction (PPI) lists for K13, EPS15, and clathrin. The K13 and ESP15 and clathrin PPI lists were devoid of clathrin, suggesting that K13 functions in a clathrin-independent endocytosis pathway. To explore these and other proposed interactions we use our Consensus co-expression network data for an independent systems-level view as a way to generate new hypotheses about this cellular pathway and the mechanism of resistance for artemisinin. We find that all of K13, EPS15, and clathrin PPI lists are statistically significantly more densely interconnected with each other than expected by chance, supporting and extending the claim that these genes are involved in the same biological process, endocytosis. We also validate some additional hypotheses of Birnbaum *et al.* [7], which further validates our inferred network data, while also providing additional novel insights into the roles of K13, EPS15, and clathrin in *P. falciparum* endocytosis pathways.

Results and discussion

Inferring networks for better functional prediction

We consider four network inference methods to infer respective co-expression networks (Section *Inference of gene co-expression networks*). Each network is referred to based on its inference method name, i.e., MI, absPCC, RF, and AdaL. Among these, AdaL is the smallest network with a density of 0.09%, indicating a conservative network inference method with few gene pairs that have strong co-expression relationships (edges). The absPCC and RF networks are dense and capture more inclusive representations of the co-expression relationships of gene pairs, i.e., absPCC has 4,322 nodes and 951,347 edges with a density of 10.19%, and RF has 4,374 nodes and 868,105 edges with a density of 9.08%. However, real-world networks are much less dense [4]. So, we aim to examine whether we can remove some proportion of the edges without disconnecting many of the nodes from the given network, as such edges could be viewed as redundant. We do this by systematically thresholding these two networks by keeping 1-100 percent of most important edges (edges with highest weights) among all of the edges in a given network. Then, for each threshold, we calculate the corresponding percent of nodes preserved in the largest connected component of the given network. Next, we take three such weight thresholds at which the resulting subnetworks do not lose many nodes in their largest connected components (Section "*Methods*"). We find that by keeping 30%, 40%, and 50% most important edges in the absPCC network, the resulting subnetworks' largest connected components contain at least 87% of all nodes in the absPCC network. We refer to these three absPCC-based subnetworks as absPCC-0.3, absPCC-0.4, and absPCC-0.5, respectively. Similarly, by keeping 3%, 5%, and 10% most important edges from the RF network, the resulting subnetworks' largest connected components contain at least 95% of all nodes in the RF network. We refer to these three RF-based subnetworks as RF-0.03, RF-0.05, and RF-0.1. Supplementary Fig. S1 illustrates the rationale for determining the number of edges kept. Therefore, up to this point, we have constructed 10 networks, one inferred using MI, four inferred using absPCC, four inferred using RF, and one inferred using AdaL.

Edge overlaps between inferred networks

Given co-expression networks constructed using the four inference methods (i.e., MI, absPCC, RF, AdaL), we examine their pairwise edge overlaps to ascertain their complementarity or redundancy. Note that for absPCC and RF, we take the smallest subnetwork (i.e., absPCC-0.3 and RF-0.03) to ensure the network includes the fewest redundant edges. For MI, absPCC-0.3, and AdaL, 46%-85% of edges are unique to the given network. The fourth network, RF-0.03, is mostly redundant to the other three networks, i.e., only 19.13% of its edges are unique (Fig. 2). Also, only 730 edges that are common to all four co-expression networks (Fig. 2). This indicates

that the co-expression networks are largely capturing different aspects of *P. falciparum* biology. For example, all co-expression networks are predicting complementary gene-GO term annotations, see below. This observation is consistent with results from other systems where different methods have been used to infer co-expression networks [43, 56]. Previous studies in other systems have shown that constructing Consensus networks from co-expression networks built with different types of inference methods can more accurately capture regulatory relationships between genes, with different networks more accurately capturing different types of regulatory interactions [43].

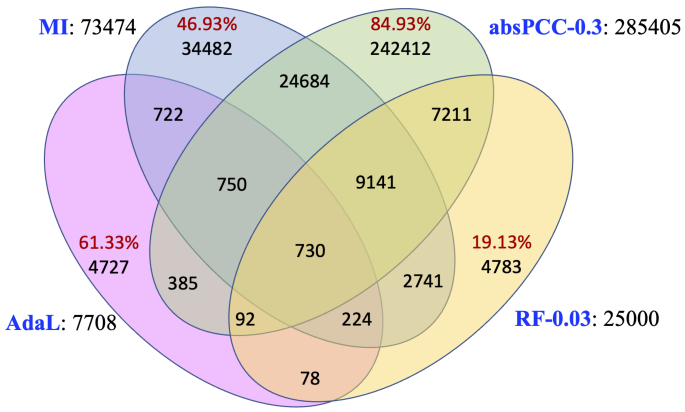

Figure 2. The edge overlaps between the four networks. Each network's name is colored in blue, and is followed by its corresponding number of edges. Within the Venn diagram, each red number is the percentage of all edges in its corresponding network that are unique to the given network. For example, out of all 7708 edges in AdaL, 4727 (i.e., 61.33% of) edges are unique to AdaL. More detailed information can be found in Supplementary Fig. S2.

To examine whether combining edges from the four networks would predict the union of gene-GO term annotations made by each individual network, we construct a Consensus network using the union of edges from the four networks. Because each of the four networks may be capturing different aspects of *P. falciparum* co-expression relationships we want the Consensus network to capture strong co-expression relationships from each network and co-expression relationships that are common to many networks. Such a Consensus network preserves the edge weights (representing the strength of their co-expression relationships) across four networks inferred from different methods. Specifically, we define a weight range across the four networks and utilize min-max normalization to normalize the weights to [0,4] range, means that more networks support an edge or that the edge is supported with a higher weight in the given network(s) (or both). So, a higher weight represents a higher edge confidence (Section "*Methods*"). Therefore, in total, we consider 11 co-expression networks in this study (10 networks constructed using the four network inference methods, plus the Consensus network). We list their sizes in Table 1.

Table 1. The 11 considered co-expression networks and their size and density statistics.

Network	# of nodes	# of edges	Density
MI	4,373	73,474	0.77%
absPCC-0.3	3,792	285,405	3.97%
absPCC-0.4	3,993	380,539	4.77%
absPCC-0.5	4,126	475,674	5.59%
absPCC	4,322	951,347	10.19%
RF-0.03	4,188	25,000	0.29%
RF-0.05	4,323	43,406	0.46%
RF-0.1	4,372	86,811	0.91%
RF	4,374	868,105	9.08%
AdaL	4,082	7,708	0.09%
Consensus	4,374	333,162	3.48%

Selecting the best clustering parameters for the inferred networks

Two clustering methods (i.e., BigCLAM (BC) and MCL) were used for each of the 11 co-expression networks to generate clusters for predicting gene-GO term associations. For unbiased evaluations of each network, we test multiple parameters by varying them for each of the two clustering methods. Then, three parameters per clustering method were systematically selected based on three criteria: i) the highest precision from cross-validation; ii) the largest coverage of unique genes in all significantly enriched clusters; iii) the largest coverage of unique GO terms in all significantly enriched clusters. These three criteria maximize the coverage of gene-GO term annotations for each network and clustering method. Note that some of the networks end up with less than three parameters being selected from the criteria because two or more criteria can have the same clustering parameter, (Section "*Methods*") (Table 2).

Table 2. The best clustering parameters for each of the three criteria, for BC and MCL, for each co-expression network. The parameters of BC (range from 25 - 700) represent the expected number of resulting clusters. The parameters for MCL start with an "I" (range from 1.2 to 5), representing the concept of inflation in MCL. Intuitively, the higher the inflation, the more clusters hence the smaller size per cluster that MCL returns. For details about each Criterion, see "Methods".

Network	BC parameters			MCL parameters		
	Criterion i)	Criterion ii)	Criterion iii)	Criterion i)	Criterion ii)	Criterion iii)
MI	425	25	450	I2.4	I1.6	I1.7
absPCC-0.3	350	100	450	I1.5	I2.9	I2
absPCC-0.4	650	125	500	I1.6	I2.3	I2
absPCC-0.5	650	275	475	I1.32	I2.6	I2.4
absPCC	650	225	225	I3.6	I2.5	I3
RF-0.03	700	25	200	I2.8	I1.2	I2
RF-0.05	600	50	350	I3.2	I1.24	I19
RF-0.1	700	50	450	I5	I1.28	I2.1
RF	475	50	75	I5	I1.7	I2.5
AdaL	550	25	75	I1.24	I1.2	I1.7
Consensus	275	275	200	I5	I1.36	I1.7

According to the selected parameters presented in Table 2, we find that there is no defining pattern of ideal parameter(s) for a clustering method because there is not a strong relationship observed between cluster size and GO term enrichment. This stresses the need of testing multiple parameters for a given clustering method.

Validating the inferred networks by predicting gene-GO term associations

For each network, we systematically select up to three clustering parameters based on our selection criteria. Then, for a given network, we evaluate each selected clustering-parameter combination to determine if clusters are enriched for genes annotated with shared GO terms and select the best clustering-parameter combination(s) using leave-one-out (LOO) cross-validation. Intuitively, given a gene g, we hide its GO term annotations. Then we examine whether each of the clusters that gene g belongs to is statistically significantly enriched in ground truth GO terms using the hypergeometric test. If such a cluster is statistically significantly enriched for GO term j, we predict gene g being annotated by GO term j. We iterate over all genes in the gene expression data and estimate prediction accuracy for each clustering-parameter combination in terms of precision and recall by comparing predicted and ground truth gene-GO term associations. Finally, we select a clustering-parameter combination for further analysis if its precision and recall are both higher than other parameters. If different clustering-parameter combinations have the highest precision and recall we select both for further analysis (see

"*Methods*"). Parameter selection based on LOO precision and recall from up to six parameters of each network is presented in Table 2 and Supplementary Figs. S3 to S7.

After the best clustering parameters are identified, we visualize the precision and recall for the selected network-cluster-parameter combinations (Fig. 3). We observe that as precision increases, the recall decreases as expected given the trade-off between precision and recall. Precision is typically favored over recall in biomedicine [38, 39] because it is more important to be correct (e.g. 9 out of 10) than inclusive (e.g. 20 out of 50) in applying these predictions. The recall of all networks and their corresponding clustering-parameter combinations are below 15%, but some of the networks yield high precision, e.g. MI yields a precision score of 86.7%n (Fig. 3). AbsPCC-0.5 follows MI closely with a precision score of 77.8%. RF-0.03 follows absPCC-0.5 with a precision score of 74.3%. Finally, AdaL follows RF-0.03 with a precision score of 56.2%. In other words, the top-performing four network-clustering-parameter combinations cover co-expression networks constructed using the four inference methods, meaning all inference methods statistically capture extensive gene-GO term annotations. On the other hand, low recall indicates that none of them capture a large fraction of all existing gene-GO term annotations.

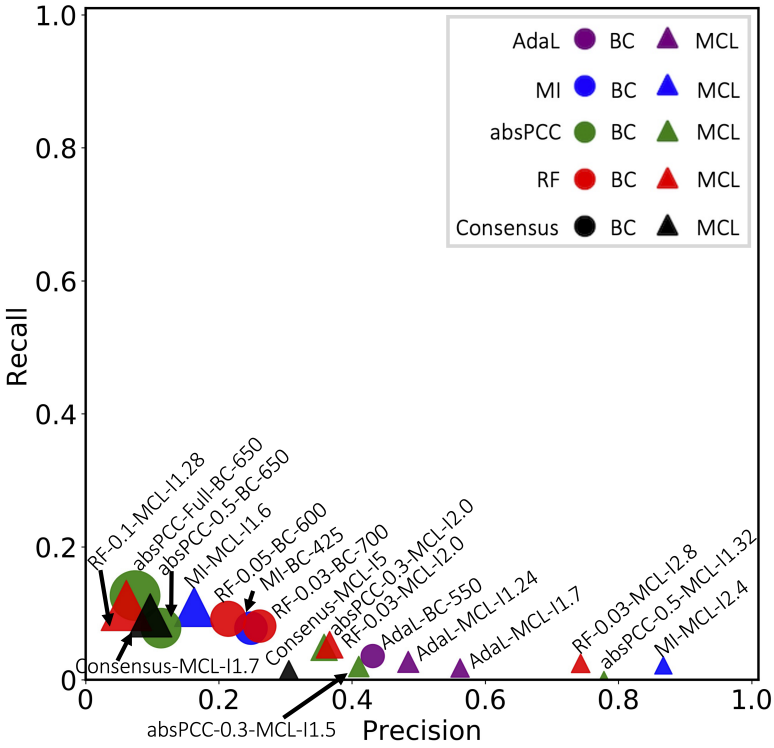

Figure 3. The prediction accuracy in terms of precision and recall from leave-one-out cross-validation. Each point is a network-clustering-parameter combination. The size of each point represents the number of predictions made by its corresponding combination the combination. The color of a point corresponds to a network, and the shape of a point corresponds to a clustering method. For example, all purple points correspond to AdaL, and among all purple points, circles correspond to BC and triangles correspond to MCL. Note, we use the same color for absPCC with different thresholds and we use the same color for RF with different thresholds.

The Consensus network that captures interactions from each of the four co-expression networks does not perform the best. In fact, it performs poorly compared to most of the other network-clustering-parameter combinations. This was shocking to us. This could be because when we integrate all edges, we introduce noisy signals into the Consensus network. This could

also be because our interaction integration algorithm does not fully preserve the interaction importance across different networks. To improve this, a better integration algorithm is needed. Importantly, even though the Consensus network does not perform the best, it does capture drug resistance "biology" relevant to endocytosis (Section "*Endocytosis-related biological signatures are captured by the Consensus network*").

Because the top-performing network-clustering-parameter combinations cover all four network inference methods, we further examine whether their predicted gene-GO term associations are complementary (i.e., unique) or redundant by examining their pairwise overlaps of predicted gene-GO term associations with respect to defined true associations vs. novel associations. Also, because the Consensus network is assumed to cover more information, we examine whether its best clustering-parameter predicts associations that are complementary or redundant to the top-performing combinations. That is, we examine the pairwise prediction overlaps for MI-MCL-I2.4, absPCC-0.5-MCL-I1.32, RF-0.03-MCL-I2.8, AdaL-MCL-I1.7, and Consensus-I5 with respect to true positives (Figs. 4) as well as novel predictions (Figs. 5). In total, these combinations predict 169 true positive and 174 novel gene-GO term associations, respectively. Among the 169 and 174 associations, 109 and 131 are unique with respect to genes, and 14 and 26 are unique with respect to GO terms. Indeed, we find that all Jaccard indices are low (the largest index is only 27%) indicating the predictions are complementary to each other. This observation strengthens our conclusion that different network inference methods capture different aspects of biological information. Importantly, despite the Consensus network not performing well compared to other networks in term of precision, it uncovers gene-GO term annotations not found by other networks.

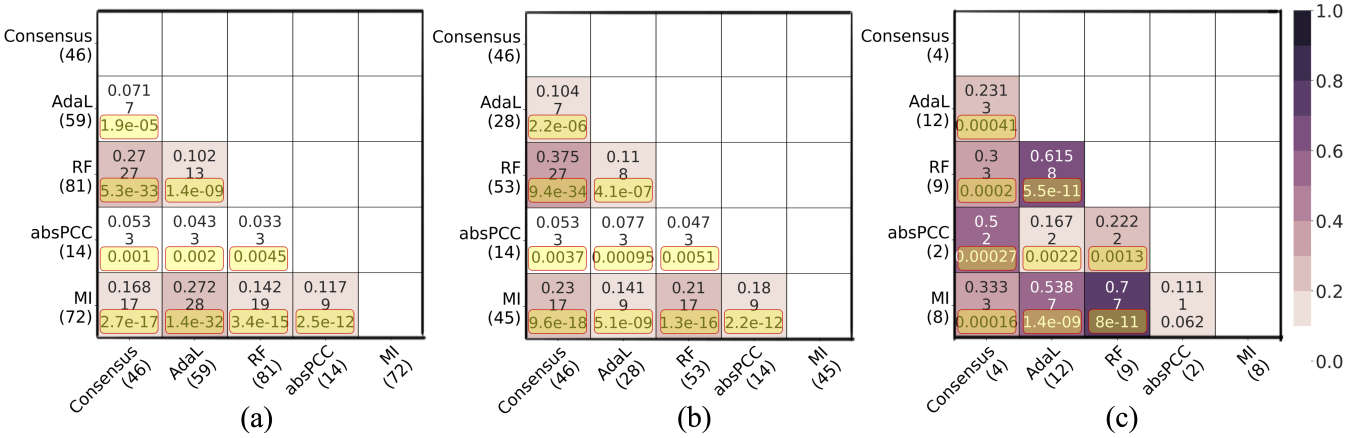

Figure 4. Pairwise overlap between predictions made by the best combination for each of the five networks with respect to **true positives**. Panel (a) represents the pairwise overlap of gene-GO term associations. Panel(b) represents the pairwise overlap of unique genes among gene-GO term associations. Panel (c) represents the pairwise overlap of unique GO terms among gene-GO term associations. Within each panel, the number under each network name represents the number of corresponding true positives. Within each cell, there are three numbers, the first number is the Jaccard index, the second number is the raw overlap count of two corresponding combinations of the cell, and the third number is the adjusted p-value resulting from the hypergeometric test. We use yellow boxes to highlight the adjusted p-values for those cells with overlaps that are statistically significant.

Ranking predicted gene-GO term associations interactions

Moreover, for each gene-GO term association, we determine the associated p-value for whether the cluster that a gene belongs to is significantly enriched with that GO term. Consequently, the more network and cluster combinations that support a gene-GO term association prediction, provides more confidence (smaller p-value) the more confidence we have for the gene-GO term assignment (see"*Methods*"). We provide two gene-GO term associations lists based on these

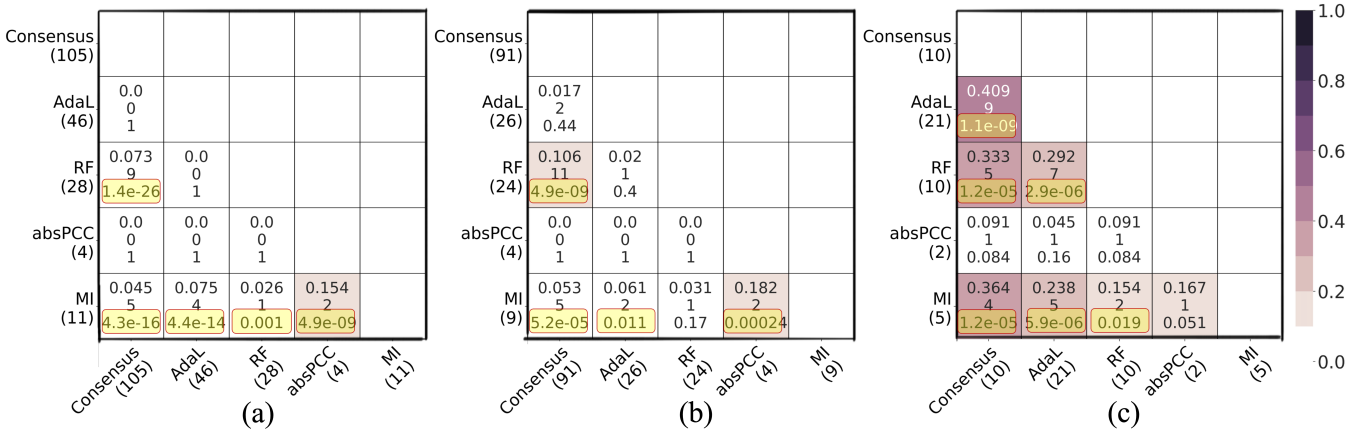

Figure 5. Pairwise overlap between predictions made by the best combination for each of the five networks with respect to **novel predictions**. Panel (a) represents the pairwise overlap of gene-GO term associations. Panel (b) represents the pairwise overlap of unique genes among gene-GO term associations. Panel (c) represents the pairwise overlap of unique GO terms among gene-GO term associations. Within each panel, the number under each network name represents the number of corresponding novel predictions. Within each cell, there are three numbers, the first number is the Jaccard index, the second number is the raw overlap count of two corresponding combinations of the cell, and the third number is the adjusted p-value resulting from the hypergeometric test. We use yellow boxes to highlight the adjusted p-values for those cells with overlaps that are statistically significant.

confidence scores ranked using true gene-GO term associations that are currently in the ground truth data (Additional File 2) as well as novel gene-GO term associations, i.e. predicted by our networks but not currently in existing database of gene-GO term associations (Additional File 3). We visualize the distribution of confidence scores with respect to true positives and novel predictions (Fig. 6). In particular, among 11 networks $\times$ 2 clustering = 22 combinations, we observe 1,062 currently known gene-GO term associations and 28,826 novel gene-GO term associations. We then visualize how well each of these 22 network-clustering combinations captures the known gene-GO term associations by pathway in Fig. 7. We find that many of the 22 network-clustering combinations appear to correctly capture pathogenesis related gene-GO term associations. However, for other GO terms different network-clustering combinations predict different gene-GO term associations.

Ranking predicted gene-gene interactions

Our systematic evaluation framework allows us to assign confidence scores to each pair of gene-gene interactions. To do so, similar to how we assign confidence scores to gene-GO term associations, we do so for edges that are present in all of the statistically significantly enriched clusters by aggregating the adjusted p-values of the enriched clusters, see *"Methods"* for methodological detail. Then, we rank the gene-gene interaction list according to their confidence scores from high to low (Additional File 4). Such a ranked list includes 1,018,420 gene-gene interactions based on their confidence score. We also visualize the distribution of confidence scores of gene-gene interactions (Supplementary Fig. S8). This list can be referenced by the malaria community, i.e., gene-gene interaction networks can be extracted from the list by using a pre-defined threshold. We anticipate these ranked gene-gene interactions will contribute to network/functional inference for *P. falciparum*.

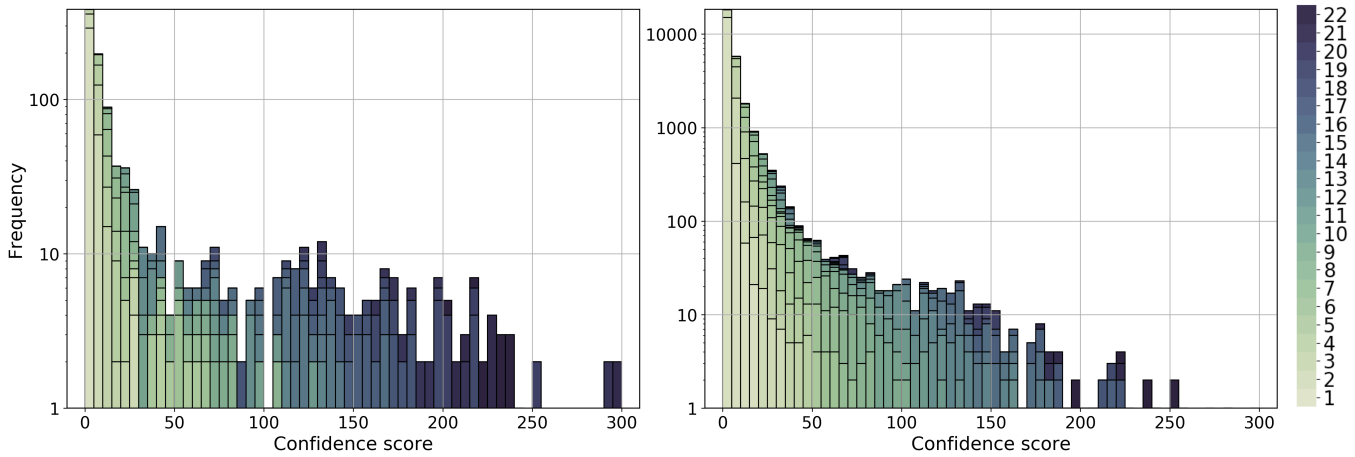

Figure 6. The confidence score distribution of predicted gene-GO term associations. The left panel shows the confidence score distribution for true associations (i.e., predicted as associations and also in ground truth data) and the right panel shows the confidence score distribution for novel associations (i.e., predicted as associations that are not currently known to be true). The color shades represent the number of network-cluster combinations that support the corresponding association. The darker color is, the more network-cluster combinations support it. The confidence score of a given gene-GO term association is calculated by aggregating the negative log of adjusted p-values from the network-clustering combinations that the gene-GO term association is supported by.

Validating the inferred networks using Endocytosis-related biological signatures

Endocytosis is an essential biological process for trafficking extracellular material in the cell to specific organelles. Extracellular material is first brought into the cell in early endosomes that mature into late endosomes as they are directed to lysosomes or through trafficking pathways from the Golgi apparatus. Kelch13 (K13) and EPS15 localize to the periphery of the cell and are suggested to contribute to the generation of early endosomes. Clathrin has been shown to function in *Plasmodium* and other apicomplexa in an atypical role, primarily through trafficking pathways of the Golgi apparatus [20, 54]. A recent study [7] identified PPIs for K13, ESP15 and clathrin. The K13 and EPS15 PPI lists are devoid of clathrin suggesting K13 functions in a clathrin-independent endocytosis pathway. Our transcription co-expression networks provide a systems level perspective on these recently published data, including new hypotheses for further exploration into this cellular pathway and the mechanism of resistance for artemisinin.

We measure how densely the K13, EPS15 and clathrin PPI lists are connected in the Consensus network. We measure the density of connections between members of each list, the union of each pair of lists and the union or all three lists. Note that, there are a few genes that are related to multiple endocytosis gene groups. We do not consider such genes because these genes could potentially mix the biological signatures that each endocytosis group captures.

Also, we find that the K13 PPI list is the most densely connected list, followed by the union of the K13 and EPS15 PPI lists (K13-EPS15), then the union of the K13 and Clathrin PPI lists (K13-Clathrin), and finally the union of all three PPI lists (All-Endocytosis) (Fig. 8). The K13 and the K13-EPS15 PPI lists are expected to be densely connected in the network, indicating the Consensus network identifies expected pathways and their interacting proteins. The dense networks between the K13-Clathrin PPI list is a more interesting result because K13 does not directly interact with Clathrin and it would not necessarily be expected that the K13 and Clathrin PPI lists share the same network. The majority of the material imported by the K13-defined endocytosis pathway is host cell hemoglobin, which is eventually transported to the food vacuole, a lysosome like structure where hemoglobin is degraded. It is plausible to hypothesize that endosomes generated by K13 are integrated into the trafficking network

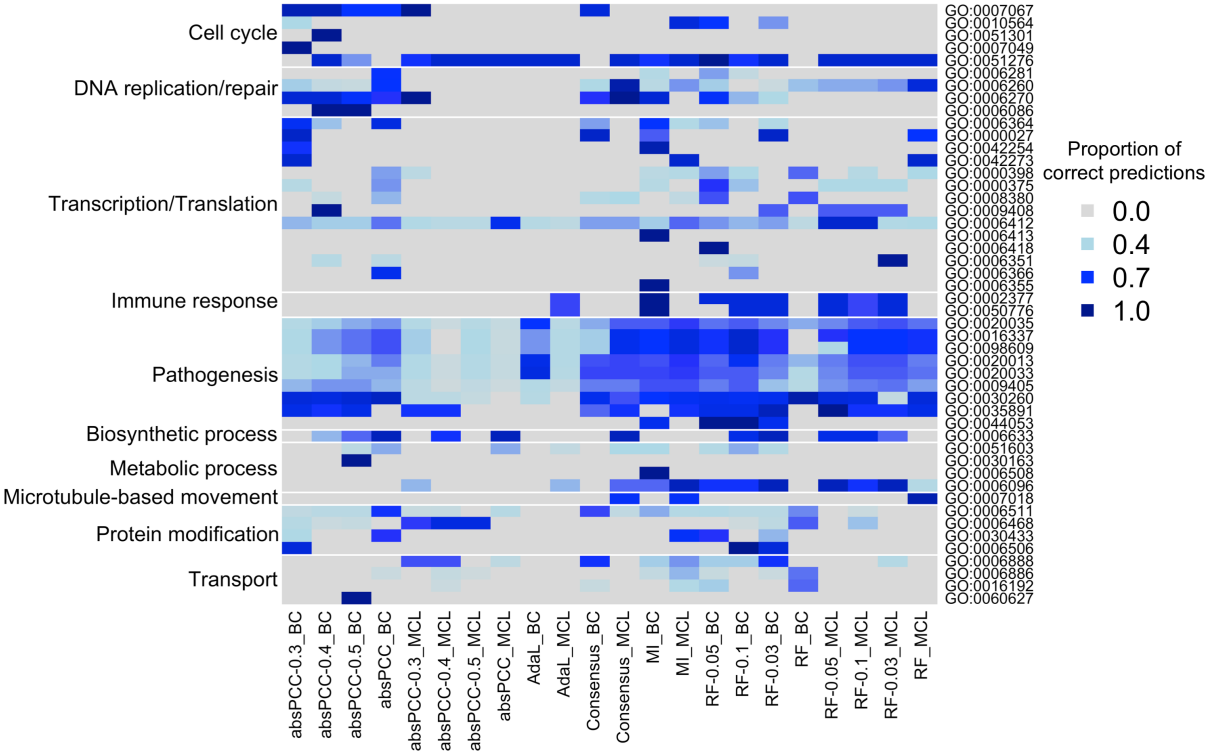

Figure 7. Network coverage of correctly predicted ground truth gene-GO term associations for each network-clustering combination. The proportion of all correctly predicted gene-GO term associations for each GO biological process in the ground truth (rows) that are correctly predicted by a given network_clustering combination (columns) are shown in shades of blue with darker blues indicating a higher proportion of gene-GO term associations are captured by a particular network-clustering combination. GO terms are grouped using semantic similarity. See Section *"Methods"* for detail.

coordinated by Clathrin and its interacting proteins through the Golgi, a result that would suggest the separate gene functions in related biological pathways even though they do not directly interact with each other.

Many of the most significant PPIs for K13 and EPS15 from Birnbaum *et al.* [7] have overlap genes. We further examine the K13, EPS15 and clathrin PPI lists by removing overlapping genes. As such, this would produce denser networks and would increase the connectivity and significance of the K13, K13-EPS15, K13-Clathrin, and all-endocytosis PPI lists. This indicates that the non-overlapping PPI of K13 and EPS15 still play an important role in the K13 defined endocytosis pathway. This further suggests the three PPI lists have potential to be operating together in the endolysosomal system to bring material into the cell and transport the material to its destination farther in the cell. Our analysis provides deeper, testable extensions of the observed PPI data for how K13, EPS15 and Clathrin are functioning as a system beyond what can be learned from only considering directly interacting protein partners.

Interestingly, the PPI lists for EPS15 and Clathrin are not statistically significantly connected when analyzed separately from the K13 PPI list either in their entirety or when overlapping genes are removed. This fits a scenario of EPS15 and Clathrin having pleiotropic functions and operating in multiple pathways. It is likely that the global transcript data used for the networks does not capture the broad spectrum of interacting partners either protein has throughout the complex *P. falciparum* cell cycle. Analyzing the lists together provides greater context to specific functions in the cell cycle when K13 is essential for cell development.

Co-expression networks for specific stages of the *Plasmodium* cell cycle could further define the multiple functions EPS15 and Clathrin preform in the cell. Endocytic mechanisms in *Plasmodium* falciparum have not been fully elucidated and are an important area of research [61]. Birnbaum *et al.* [28] is a significant step in understanding how K13 functions inside the cell and suggests K13 and Clathrin perform different functions inside the cell in separate pathways. Our data suggests the functional pathways for K13 and Clathrin are more correlated than would be expected by only the PPI found in Birnbaum *et al.* [28]. Further molecular experiments will provide greater context for how the two functional pathways are coordinated and influence artemisinin resistance.

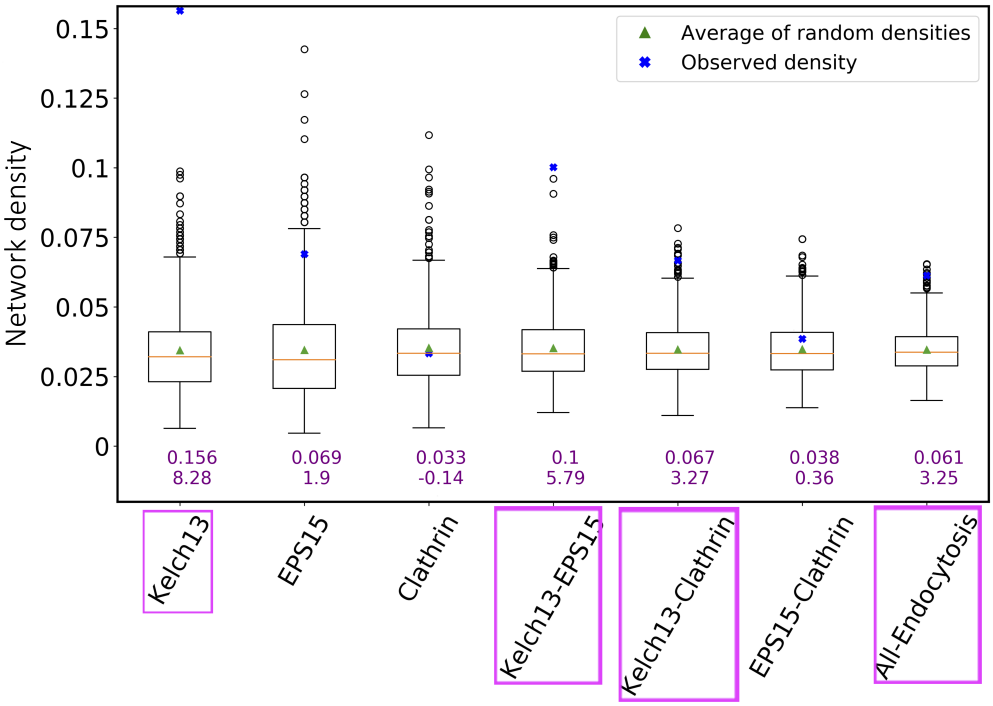

Figure 8. The connectivity of endocytosis gene groups compared with connectivity expected by chance. The x-axis is different endocytosis-related gene groups. The y-axis is network connectivity measured by network density. The boxplot for a given group represents the density distribution of 1000 random runs for each endocytosis gene group. In particular, if a given gene group has z genes, the connectivity by chance is measured by calculating the density of a subnetwork consisting of randomly selected z genes from the Consensus network. The green triangle for each group is the average densities of 1000 randomly selected subgraphs. The orange line in each box is the medium of random densities. The blue cross point for each group is the observed density of its corresponding endocytosis gene group. The two purple numbers under each boxplot are the observed density and the z-score. The pink boxed endocytosis groups are those groups that are significantly densely connected than at random.

Conclusions

In this study, we have inferred gene co-expression networks using four prominent network inference methods of *P. falciparum* genes. Then, we have utilized the inferred co-expression networks to predict known and novel functional annotations of *P. falciparum* genes. We systematically evaluated how accurately these networks perform. Our results show that different networks capture complementary aspects of co-expression relationships. Thus, relying on a single inference method should be avoided when possible.

We have also demonstrated how these inferred gene co-expression networks can be used to explore connectivity of gene lists using recently published PPIs for three endocytosis-related genes (i.e., kelch13, EPS15 and clathrin PPI lists) [7]. We find that the Kelch13, EPS15, and clathrin PPI lists combined are statistically significantly more densely interconnected with each other than expected by chance.

Methods

Data

Gene expression data

The gene expression data (available from GEO as GSE19468) we use to construct our co-expression networks was generated by Hu *et al.* [21] in 2009, as follows. Drug perturbations were conducted for 29 drugs across 10 experimental groups (each with a no drug control and two - four drugs, see Table 3) and samples were collected at five - ten time points across the *P. falciparum* intra-erythrocytic developmental cycle. This experiment resulted in *P. falciparum* transcription profiles for 247 samples. Transcript abundance levels were obtained using a spotted oligonucleotide microarray [22] with 10,416 probes representing the 5,363 genes in the PlasmoDB *P. falciparum* genome version 4.4. In this unprocessed dataset probes are in rows and samples in columns. There have been major revisions in subsequent PlasmoDB *P. falciparum* genome versions. So, rather than using the processed transcription profiles directly, we reprocessed the probe level data to better reflect genome updates and improved normalization methods.

Table 3. The information about drug treatments and time courses of GSE19468. For example, group 1 has eight time courses for one control group and three drug treatments. That is, there are $8 \times 4 = 32$ gene expression levels for a given gene obtained from group 1. By combining the expression levels across all groups, in total, there are $8 \times 4 + 5 \times 4 + 7 \times 5 + ... + 10 \times 3 = 247$ gene expression levels for each of the 5,075 genes. Of which, $8 + 5 + 7 + ... + 10 = 64$ gene expression levels are from control treatments.

Group	Time Points	Treatments
1	8	Control, RoscovitineA, CyclosporineA, FK506
2	5	Control, Colchicine, Na3VO4, StaurosporineA
3	7	Control, ML7, W7, KN93, Staurosporine
4	6	Control, Artemisinin, Chloroquine, Febrifugine, Quinine
5	5	Control, E64, Leupeptine, PMSF, RetinolA
6	6	Control, Apicidin(troph 5nM), Apicidine(troph IC90)
7	5	Control, Apicidin(schiz IC50), Apicidin(schiz IC90)
8	6	Control, TrichostatinA(IC50), TrichostatinA(IC90)
9	6	Control, Chloroquine(IC50), Chloroquine(IC90), Chloroquine(2*IC90)
10	10	Control, EGTA(IC50), EGTA(IC90)

Processing probe-level data

To reflect revisions to the *P. falciparum* genome since 2009, nucleotide sequences for the 10,416 probes on the spotted array were obtained from GEO (GPL7493) and were aligned to the PlasmoDB *P. falciparum* genome version 36 using blast+ (v2.6.0) from NCBI. The 9,870 probes that aligned the *P. falciparum* transcriptome (PlasmoDB v36) with perfect match (bitscore ¿= 130) and no secondary alignments (secondary bitscores all ¡ 60) were retained in the dataset. These probes aligned to transcripts for 5,075 genes. Probes aligned to transcripts for the same gene were averaged and genes with non-zero values in ¿ 80% of samples were retained in the dataset. This data processing introduced missing values into the dataset. After blast mapping,

we end up with 4,503 genes with gene names updated in our gene expression data (Additional File 5 - GSE19468_blasted.csv).

Imputing missing values in the gene expression data

Some of the network inference methods utilized in this study cannot be used when the underlying gene expression data contain missing data e.g., absPCC, thus it was necessary to impute these missing values. We test seven prominent imputation methods designed for gene expression data. Then, we select the method that performs the best in the expression data used in this study. By "best", we mean the method that yields the smallest normalized root mean squared error (NRMSE). In particular, NRMSE is calculated as $\frac{\sqrt{mean[(\hat{y}-y)^2]}}{std(y)}$, where $\hat{y}$ represents the imputed values and y represents the actual values. The seven prominent imputation methods are explained as follows.

- Multiple imputations by chained equations (MICE) [8] imputes a column (i.e., experiment) by modeling each experiment with missing values as a function of other experiments in a round-robin fashion. That is, given an experiment column of interest, namely, y, and all other experiment columns, namely X. A regressor is then fitted on X and y by learning a regression model from known values in X and y to predict the missing values in y.

- SVDimpute [69] is a singular vector decomposition (SVD)-based imputation method. Intuitively, a matrix can be recovered asymptotically by only using the significant eigenvalues. That is, given a gene u, a regression model of gene u and k most significant eigenvalues (i.e., eigengenes) are fitted. Then, the learned coefficients of the linear combination of the k eigengenes are used to impute the missing values of gene u. The processes are repeated iteratively until all missing values were imputed.

- KNNimpute [69] imputes the missing values as follows. First, given a gene u with a missing value in experiment j, k other genes that are most similar to gene u that have expression values in experiment j are selected. Then the weighted average of value in experiment j from the k selected genes is treated as an estimated expression level for gene u in experiment j, where the weight is based on the expression similarity of a gene (i.e., among the k selected genes) to the gene u. The expression similarity between two genes is measured using Euclidean distance. We vary k from 1 to 24 with an increment of 2.

- Local least squares imputation (LLSimpute) [29] imputes the missing values as follows. First, k other genes that are most similar to gene u of interest are selected. By most similar, we mean these k genes have the largest absolute Pearson correlation coefficients with gene u. It differs from KNNimpute (i.e., k is predefined) that the k value for LLSimpute is introduced automatically.

- SoftImpute [45] imputes the missing values by guessing values repeatedly. Specifically, the missing values in the gene expression data were initially filled as zero. Then a guessed matrix is updated repeatedly by using the soft-threshold SVD with different regularization parameters. If the smallest of the guessed singular values is less than the regularization parameter, then the desired guess is obtained. For methodological detail, please refer to [45].

- BiScaler [19] was proposed based on SoftImpute but using alternating minimization algorithms. It introduced the quadratic regularization to shrink higher-order components more than the lower-order components such that it offers a better convergence compared to SoftImpute. For methodological detail, please refer to [19].

- NuclearNormMinimization [10] imputes the missing values by solving a simple convex optimization problem. That is, for a matrix M based on a theory that the missing values

can be recovered if the number of missing values m obeys $m \geq cN^{1.2}rlogN$, where N is the number of rows in matrix M, c is a positive numerical constant, and r is the rank of M. This algorithm usually works well on smaller matrices.

We use the library "pcaMethods" from Bioconductor R package [62] to perform LLSimpute and the python library "fancyimpute" to perform the remaining six imputation methods. We evaluate the performance of each method on our data as follows. (i) We take rows and columns without any missing values from the expression data as our ground truth data. (ii) We randomly remove 3.14% values from the ground truth data. We use 3.14% because it is the percentage of missing values in our expression data. We repeat this process five times and obtain five testing gene expression data. (iii) We apply an imputation method to each of the five testing data and compare the imputed matrix with the ground truth matrix. (iv) We select the method that yields the smallest average NRMSE across five runs. (v) Finally, we use the selected "best" method to impute the missing values for our entire gene expression data. It turns out that the MICE (with NRMSE = 0.204) is the best imputation method for our expression data.

Accounting for cyclical stage variation

P. falciparum has strong cyclical patterns of transcript expression across the intraerythrocytic development cycle (IDC) and these changes in gene expression tend to swamp other sources of transcriptional variation. To control for this strong cyclical variation we normalize each drug expression timepoint by its matched control timepoint. Since these are already log2 normalized expression profiles we subtract the control treatment from the experimental treatments for each timepoint. Specifically, for a given gene when treated by a drug, the *updated* expression level at time point t is obtained by using its *original* expression level minus the expression level at its control treatment at time point t. The resulting processed gene expression data thus has 4,374 genes and 183 (i.e., $247 - 64$) expression levels (i.e., no control groups as these are used to normalize for cyclical variation). The corresponding data is attached as (Additional File 6 - GSE19468_final.csv).

Ground truth GO term annotation data

We use GO term annotations as our ground truth data to evaluate whether a cluster is statistically significantly enriched in a GO term. GO terms describe the knowledge of the biological domain with respect to three aspects: 1) molecular function, 2) cellular component, and 3) biological process. We focus on biological process because these terms group genes related to a single objective and is closest to defining gene products involved in the same pathways. We obtain all GO terms that describe biological processes and their annotated genes from two most commonly used databases for *P. falciparum* genes, i.e., GeneDB[3] and PlasmoDB[4]. Because these two databases cover gene-GO term annotations that are complementary to each other, we combine their annotations and remove duplicates. As such, we obtain 4,736 gene-GO term associations that encompass 793 unique GO terms and 2,624 unique genes.

We use the processed data of gene-GO term associations to validate our clusters. Specifically, we treat each GO term as a ground truth cluster such that all genes annotated by this GO term belong to the same cluster. In general, a valid cluster should include at least three genes. So, we further process the ground truth data by only keeping those GO terms that annotate at least three genes in the expression data. We denote such GO terms as relevant GO terms and those associations involved with relevant GO terms as relevant gene-GO term associations. In our experiments, if we mention GO terms, we mean relevant GO terms. We summarize the statistics of our ground truth data in Table 4. The corresponding data is attached as (Additional File 7 - gene-GO term associations.txt).

[3] `https://www.genedb.org/`
[4] `https://plasmodb.org/plasmo/app`

Table 4. Statistics of relevant GO terms and gene-GO term associations.

# of genes	# of samples	# of relevant GO terms	# of relevant gene-GO term associations
4,374	183	255	3,232

Endocytosis data

PPI data used for the investigation of endocytosis related genes in the Consensus network was generated recently by Birnbaum *et al.* [7] in 2020. The study used a BioQ-ID method coupled with mass spectroscopy using asynchronous cultures to define protein-protein interactions (PPI) of three proteins either directly implicated in artemisinin resistance (kelch13) or as controls (EPS15 and clathrin) to fully investigate the molecular function of resistance genes. Initially the PPI of kelch13 (k13) (i.e., the molecular marker for artemisinin resistance) were identified and a subset were confirmed by cellular localization by immunofluorescence. The *P. falciparum* homolog of EPS15 was identified and confirmed as an interacting partner of kelch13 [68]. As such, EPS15 was chosen as a positive control for the BioQ-ID experiment and the genes identified as the PPI of EPS15 largely overlapped with genes of the kelch13 PPI list. This added further evidence *kelch13* was involved in endocytosis. The study further defined a PPI list for clathrin because it is the main structural protein for canonical endocytosis pathways. The PPI list for clathrin did not overlap with the kelch13 or EPS15 PPI lists leading to the conclusion that kelch13 functions in an endocytosis pathway devoid of clathrin. Our analysis utilizes the 173 endocytosis-related genes from the Supplementary Table 1 of [7]. The kelch13 PPI list contains 63 proteins, 60 of which are present in our gene expression data. The EPS15 PPI list contains 49 proteins, 48 of which are in the gene expression data. The clathrin PPI list contains 61 proteins, 58 of which are present in our gene expression data.

Inference of gene co-expression networks

Given the processed gene expression data (GSE19468), we apply four network inference methods, i.e., mutual information (MI) [44], absolute Pearson correlation coefficient (absPCC) [56], Random Forest (RF) [24], and adaptive Lasso (AdaL) [32]. Moreover, we construct a Consensus co-expression network by taking the union of networks inferred using these four methods. In this section, we explain how we infer these co-expression networks.

Network construction using ARACNe framework

We use ARACNe framework for three network inference methods: MI, absPCC, and RF. Specifically, MI quantifies the mutual dependence (either linear or non-linear) of two random variables, and absPCC quantifies the linear correlation between two random variables, see [56] for detail. RF [24] is a tree-based method aiming to recover a network involving n genes into n subproblems such that each subproblem recovers the regulation relationship of a given gene. We use the python program "GENIE3" to find the edge weight of each gene pair. For methodological detail, see the original publication [24].

Network construction processes of a network include weighting co-expression relationships for each node pair and finding an appropriate threshold to distinguish between edge and non edge. However, finding an appropriate weight threshold for real-world networks is challenging [56]. Different weight thresholds lead to different networks, hence different network topological structures [57]. Because our goal in this study is not to examine the effect of various weight thresholds but to uncover novel functional knowledge about *P. falciparum* using networks. So, we choose a well-established network construction framework called ARACNe [44] to construct three networks based on the aforementioned three edge weight strategies. ARACNe was originally proposed to infer gene regulatory networks, and has been successfully applied to infer gene co-expression networks [2, 3, 46, 60, 70]. ARACNe first calculates an appropriate threshold

I_0 based on an null hypothesis that gene pairs are independent to each other if their mutual information is below I_0. Then network construction by ARACNe was conducted by first generating 100 bootstraps from the expression data. In each bootstrap, a certain number of microarray samples (i.e., in our case 183) for all genes are randomly selected with replacement and are permuted. Then, a network using mutual information is constructed and pruned using the pre-calculated threshold I_0 and data processing inequality (DPI). In particular, given a triangle subgraph (i.e., genes $g1$, $g2$, and $g3$), DPI removes the edge with smallest weight in the triangle. Intuitively, this is because in this example, $g1$ and $g3$ are interacting with each other indirectly (i.e., through $g2$) and hence should be removed. Finally, the final network is obtained by keeping those edges that are detected across 100 bootstraps statistically significant amount of times. In other words, only non-random gene pairs are kept (i.e., adjusted p-values < 0.05 using false discovery rate (FDR) correction). For methodological detail, please refer to the original publication [44].

We directly apply the ARACNe-AP implemented by Lachmann *et al.* [33] to construct our MI co-expression network. For absPCC, we set the I_0 to 0.6 according to [9, 27] that two metabolites with Pearson Correlation Coefficients ≥ 0.6 are considered as associated. Then we follow the ARACNe framework to obtain our final absPCC network using 100 bootstraps and the DPI technique. For RF, because the tree-based method includes a pruning step which functioned as a weight threshold, we do not set the threshold I_0. Instead, we directly adopt the GENIE3 implementation from the original publication [24] and the DPI technique for each of the 100 bootstraps. Finally, we use the FDR correction from ARACNe framework to obtain the final RF co-expression network.

Because the resulting absPCC and RF networks are still very large, we further threshold these two networks by keeping k% most important edges out of all edges in the network without disconnecting the network (i.e., losing too many nodes in the largest connected component). We vary the k from 1-100 and select three such thresholds for each of the absPCC and RF networks. Thus, from this process, we obtain nine networks, i.e., four absPCC-based co-expression networks, four RF-based co-expression networks, MI co-expression network.

Network construction using Adaptive Lasso

Graphical Gaussian Models (GGMs) are prominent methods for modeling gene associations based on microarray gene expression data [12, 37, 59, 75]. GGMs are often used to obtain unbiased estimate of partial correlation between gene i and gene j, such that the partial correlation coefficient is treated as the edge weight of gene i and gene j in the resulting network. GGMs suffers two limitations, (i) they assume that the number of microarray experiments is much larger than the number of genes to ensure that the inversion of the covariance matrix in GGMs can be assessed statistically; (ii) they calculate partial correlation coefficients for all gene pairs in the expression data without a threshold. However, (i) the real-world gene expression data usually comes with a larger number of nodes compared to the number of microarray experiments; (ii) only those gene pairs with strong correlations (i.e., correlations coefficient greater than a certain threshold) are meaningful. To address such limitations of GGMs, Krämer *et al.* [32] proposed AdaL, a GGMs-based method that uses Lasso penalty to shrink the small edge weights (i.e., coefficients) to zero by using L1 norm regularization, i.e., Lasso. This way, those edges that are not meaningful will be shrunk to zero, i.e., removed from the resulting network. As such, those gene pairs with strong partial correlations are kept and hence form a network. For methodological detail of AdaL, please refer to the original publication [32]. Note that we do not apply ARACNe for AdaL as it already uses Lasso penalty to shrink small edge weights to zero. Thus, from this process, we construct another co-expression network, i.e., AdaL.

We use the R package "parcor" (available from the R repository CRAN) [32] to generate our AdaL network using our gene expression data. The input data is a $m \times n$-dimensional matrix where m is the number of microarray treatments (i.e., 183) and n is the number of genes (i.e., 4,374). The output is a $n \times n$ adjacency matrix of the resulting network.

Construction of the Consensus network

Co-expression networks that are inferred using different inference methods have complementary edges (Section "*Results and discussion* "). So, we aim to examine the properties of a network that is the union of four aforementioned co-expression networks, namely, Consensus co-expression network. We construct the Consensus network using MI, smallest absPCC (absPCC-0.3), smallest RF (RF-0.03), and AdaL, as follows.

1. Given that we have four networks with different number of edges. If network 1 has $x1$ edges and network 2 has $x2$ edges where $x1 < x2$. We argue that the least important edge in network 1 (ranked as $x1$) should be equally important as the edges have rank $x1$ in network 2. This is because each network is inferred via methods with well-established thresholding strategy, and a network with more edges is intuitively have a more loosen thresholding strategy compared to a network with fewer edges.

2. Because we want to make sure that the higher the rank value for an edge, the more important the edge is. For example, in network 1, an edge with rank $x1$ means the edge is the most important edge in network 1. So, we reverse the way we rank edges from step 1.

3. To assure the above two steps are satisfied when we construct the Consensus network, we first calculate the number of edges in all four networks (i.e., AdaL, MI, absPCC-0.3, and RF-0.03). If network 4 is the largest network with $x4$ edges, we use $x4$ as our possible maximum rank such that the most important edge in each of the four network has the same rank, which is $x4$.

4. According to step 3, network 1 has edge ranks from $x4$ to $x4 - x1$, network 2 has edge ranks from $x4$ to $x4 - x2$, network 3 has edge ranks from $x4$ to $x4 - x3$, and network 4 has ranks from $x4$ to 1.

5. After we get all raw ranks for edges of each network, we use min-max normalization to normalize the rank of each edge in each network. That is, we first find the maximum (i.e., max also $x4$) and minimum (i.e., min also 1) edge rank across the four networks. Then, for a given edge between gene i and j with weight w_{ij}, the normalized rank is $((w_{ij} - min)/(max - min)$. The resulting normalized rank of edges across four networks spans from 0 to 1.

6. Finally, for a given edge, we sum the weights from the four networks. The collections of all such edges forms the Consensus network. That is, an edge between gene i and j in the Consensus network has a weight of $w_{ij} = sum(w_{ijl})$ for $l = 1, 2, 3, 4$, where l is the network id. Consequently, the resulting Consensus network has a maximum possible edge weight of 4 and a minimum possible edge weight of 0.

Thus, from this process, we construct a co-expression network, i.e., Consensus. In total, we construct and analyze 11 co-expression networks in this study.

Clustering methods

Recall that we test two prominent network clustering methods (i.e., cluster affiliation model for big networks (BigCLAM, referred to as BC) [78] and Markov Clustering (MCL) [14]) to predict gene-GO term associations. BigCLAM is a soft clustering method (i.e., a node can be assigned to multiple clusters) and MCL is a hard clustering method (i.e., a node can only be assigned to one cluster). We select one method for each type to reduce the effect of clustering type towards prediction accuracy of gene-GO term associations as much as possible. Also, we test multiple clustering parameters to give each network the best case of advantage.

BigCLAM

BigCLAM (BC) is a non-negative matrix factorization-based algorithm that assumes the overlaps between communities are densely connected. It also detects densely overlapping and hierarchically nested communities. For methodological detail and implementation, please refer the original publication [78]. We apply BigCLAM to each of the 11 networks inferred in this study. Specifically, for a given network, we run the BigCLAM with different parameters, i.e., the number of resulting clusters. We vary it from 50 to 700 with an increment of 25 from 50 to 500 and an increment of 50 from 500 to 700. Note that the number of resulting clusters is pre-defined number, meaning that the actual number of clusters can be different as the parameter. Then, we test the prediction performance of each network_clustering_parameter combination, and systematically select up to three combinations based on three pre-defined selection criteria, see Section "*Predicting and evaluating function annotations from clusters*" for detail.

MCL

MCL is an efficient random walk-based algorithm that assumes nodes that are densely connected to each other are similar to each other. MCL has been widely applied to detect the modules in the networks [5, 40, 76]. It takes the adjacency matrix representation and uses expansion and inflation stochastic process the make the densely connected area denser and the sparsely connected area sparser. We apply MCL to each of the 11 networks, and vary the inflation parameters within the range of 1.2 to 5.0 (i.e., as suggested from the user manual [5]). A smaller inflation parameter tends to result in less number of clusters with bigger cluster sizes compared to a larger inflation parameter. Specifically, we test 33 inflation parameters with an increment of 0.02 for inflation from 1.2 to 1.4, an increment of 0.1 from 1.4 to 3, and increment of 0.2 from 3 to 4 and an increment of 1 from 4 to 5 for each network. Then we test the prediction performance each network_clustering_parameter combination, and systematically select up to three combinations based on three pre-defined selection criteria, see Section "*Predicting and evaluating function annotations from clusters*" for detail.

Predicting and evaluating gene-GO term associations from clusters

We establish a systematic parameter selection and evaluation framework to evaluate each of the network_clustering_parameter combinations, as follows.

1. For the given gene expression data, we use relevant GO terms to predict and evaluate the gene-GO term association prediction accuracy for each of the network_clustering_parameter combinations (i.e., we refer them as combinations for the rest of the paper).

2. For the clusters from a given combination, we use hypergeometric test (Section "*Hypergeometric test*") to compute the probability scores (i.e., p-values) of the enrichment significance between each pair of a given cluster and a GO term. If a cluster is statistically significantly enriched in at least one GO term, we mark this cluster as an enriched cluster. We test all clusters and obtain the significantly enriched clusters. Then we define our first two parameter selection criteria as follows, (1) the number of unique genes in the union of all enriched clusters; (2) the number of unique GO terms that are enriched in all enriched clusters.

3. In parallel, we make gene-GO term association predictions using significantly enriched clusters and GO terms via leave-one-out (LOO) cross-validation [58], as follows.

    - First, we hide a gene i's GO term knowledge at a time.

[5] `https://micans.org/mcl/`

- Second, we test whether each of the clusters that gene i belongs to is significantly enriched in any GO term. If such a cluster is statistically significantly enriched by a GO term j, we predict gene i annotated by GO term j.
- Third, we repeat the above two steps for every gene that has known GO term annotations. Then we use precision, recall to evaluate prediction accuracy. The precision is the percentage of correct predictions among all predictions we make. The recall is the percentage of correct predictions among all known association. Because there is always a trade-off between precision and recall, we use precision as our parameter selection criteria (3). We do this because we believe that in biomedicine, for wet lab validation of predictions, it is more important to have a high precision if we can not have both high precision and recall [38, 39].

4. According to our three selection criteria, each network_clustering combination has up to three clustering parameters. Different selection criteria could end up with the same clustering parameter. This is why we have up to three selected clustering parameters for a given network_clustering combination. Because we apply two clustering methods for each network, We end up with up to six clustering_parameter combinations for each of the 11 co-expression networks.

5. Because we also aim to compare prediction performance across different networks. We first select the best clustering_parameter combination(s) based on their LOO cross-validation precision and recall for each network. Specifically, for two combinations of interest, if combination 1 has a higher precision and a higher recall or a similar recall compared to combination 2, we select combination 1. If combination 1 has a higher precision but a lower recall compared to combination 2, we keep both. For those selected "best" combinations of each network, we further compare them using the same selection criteria to find the network_clustering_parameter(s) that yield the best prediction accuracy in terms of precision and recall.

6. Finally, we perform deep-dive analysis for those selected combination from step 5 using Jaccard index and overlap coefficient. Both methods measure the overlaps between two sets. In particular, given set A and set B, the Jaccard index is $\frac{|A \cap B|}{|A \cup B|}$, and the overlap coefficient is $\frac{|A \cap B|}{min(|A|,|B|)}$. The Jaccard index results in more accurate results when the sizes of set A and B are close to each other, while overlap coefficient results in more accurate result for small data when the sizes of set A and B are far away from each other. The number of predictions made by different combinations can be very different or similar, which is why we use both indices to quantitatively measure our deep-dive analysis.

Hypergeometric test

We perform hypergeometric test [17] for each pair of a cluster and a GO term (e.g., cluster 1 and GO term 1). Formally, the background (i.e., population) is the number of genes in the expression data of interest, represented as N. If C is a cluster, G is a GO term, x is the overlap between the cluster C and the GO term G, then the p-value is computed as: $P(X \geq |x|) = 1 - \sum_{i=0}^{|x|-1} \frac{\binom{|N|}{i}\binom{|N|-|C|}{|G|-i}}{\binom{|N|}{|G|}}$. Because we perform multiple tests, we adjust the p-values using false discovery rate (FDR) correction as follows.

- Within each network_cluster_parameter combination, assuming we have $c1$ clusters and $g1$ GO terms. We adjust $c1 \times g1$ p-values (i.e., each corresponds to a cluster and a GO term pair). We then use the adjusted p-values to determine whether a GO term is significantly enriched in a cluster.

- After we select up to six parameters per network based on our three systematic selection criteria, we recorrect up to $11 \times 6 \times c1 \times g1$ p-values (i.e., we have 11 networks) for the purpose of fairly comparison between networks for a given gene expression data. By recorrect, we mean we take the up to $11 \times 6 \times c1 \times g1$ p-values and use FDR correction to obtain the adjusted p-values. We do not correct across all tested clustering parameters because some of the parameters are tested to make sure that we are not missing some of the important clustering parameters. Therefore, adding p-values from these parameters for test correction can be too conservative, and consequently remove lots of true positives.

Assigning confidence scores to the predicted gene-GO term associations

In addition to evaluate the prediction accuracy of different networks, another main goal in this study is to predict and rank gene-GO term associations based on their confidence score. In particular, for a given gene expression data, we provide two lists of ranked gene-GO term associations, 1) true association predictions (i.e., those that from ground truth data), 2) novel association predictions (i.e., those that currently not known), along with their "confidence" scores. Intuitively, the more of the networks support an association, and the more significant the association is (i.e., the lower the adjusted p-value of the association), the more confident the association is. We rank the associations as follows.

- Recall that we have 11 co-expression networks and two clustering methods, which totals to 22 network_clustering combinations (i.e., 22 adjusted p-values). Note that we select up to three clustering parameters per network_clustering combination, each corresponds to an adjusted p-value. We select the smallest adjusted p-value as the adjusted p-value for corresponding network_clustering combination.

- We rank predictions based on the number of network_clustering combinations that support this prediction and their corresponding adjusted p-values. Specifically, we first take the negative log of the adjusted p-values (transformed p-values), such that the smaller the adjusted p-value a prediction has (i.e, the more important the prediction is), the larger the transformed p-value is. We then sum the 22 transformed p-values and get one final index for each prediction, i.e., confidence score. We rank the predictions from high to low based on their confidence scores.

To visualize how effectively each network_clustering combination is at predicting true gene-GO term associations we construct a heat map showing the proportion of gene-GO term associations correctly predicted for each GO term by a given network_clustering combination. To visualize related GO terms we assign groups using semantic similarity (REVIGO) [63].

Assigning confidence scores to the predicted gene-gene interactions

Similar to the prediction of gene-GO term associations, we also provide a reference list of gene-gene interactions (GGIs) and their "confidence" scores. Intuitively, the interactions that yield the most meaningful gene-GO term associations, are supported by most amount of the networks, and/or are among the top-scoring interactions in their respective network, will be the most confident interactions. Specifically, the rank the GGIs as follows.

- For each of the 22 network_clustering combinations, we first identify the statistically significantly enriched clusters, and get all genes in the clusters along with their edges from the network.

- For each identified edge, we assign the negative log transformed p-value associated with the cluster that the edge belongs to as its weight. If an edge belongs to multiple clusters, (e.g., genes can be grouped into multiple clusters via BigCLAM), we select the one with smallest adjusted p-value (i.e., the largest transformed p-value).

- We sum up the 22 transformed p-values (i.e., each correspond to a network_clustering combination) and get a final confidence score for each GGI. We rank the GGIs from high to low based on their confidence scores.

Examining the connectivity of endocytosis-related genes in the Consensus network

We use the Consensus network to examine the hypotheses of endocytosis process from Birnbaum *et al.* [7]. Specifically, if a network shows that the *kelch13*-related genes and *EPS15*-related genes are close to each other than at random in the network, it would corroborate the initial finding of the Birnbaum *et al.* study by a complementary analysis on independent data. We would also expect clathrin-related genes to be closer to each other than random and distant from *kelch13*-related and *EPS15*-related genes with connectivity similar to random in the network. We evaluate the connectivity of each group of Endocytosis genes using their network connectivity, i.e., the density, as follows.

- Given a group of Endocytosis genes, assume m genes, we select the induced subgraph (i.e., genes and their interactions) of the genes from a given network and we calculate the observed density of the subgraph. Network density measures how close a network is to its complete version (i.e., all pairs of nodes are connected).

- We then randomly select m genes from the network and their induced subgraph. We calculate the network density. We repeat this process a thousand times and calculate the z-score of the observed density compared to densities from the 1000 random runs.

- We use 2.0 as z-score threshold to determine whether the observed density is significantly larger than the random densities. In particular, if the z-score of a group of endocytosis genes is greater than 2.0, then the group of Endocytosis genes are densely connected than expected by chance.

Supporting Information

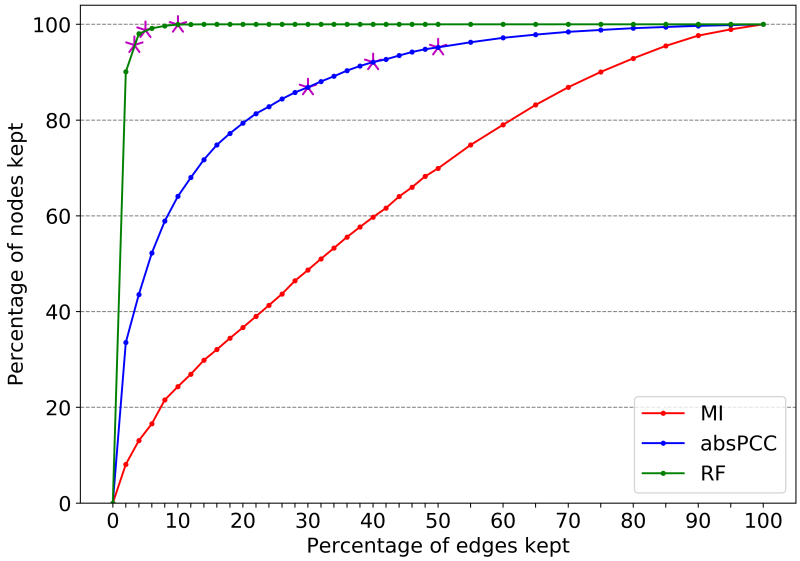

Supplementary Fig. S1. The effect of edge weight thresholds on the size of the largest connected component for a given network. It illustrates the percent of nodes remained in the largest connected component out of all nodes in a given network when keeping $k\%$ of highest weighted edges in the given network (i.e., MI, absPCC, RF). The x-axis represents the percent of highest weighted edges kept (i.e., $k\%$) out of all edges in a given network. The y-axis represents the corresponding percent of nodes remained in the largest connected component out of all node in the network when keeping $k\%$ highest weighted edges. k is varied from 1 to 100. The magenta stars indicate the three thresholds we select for absPCC and RF, respectively. Note that we include MI in the figure as a control visualization for absPCC and RF.

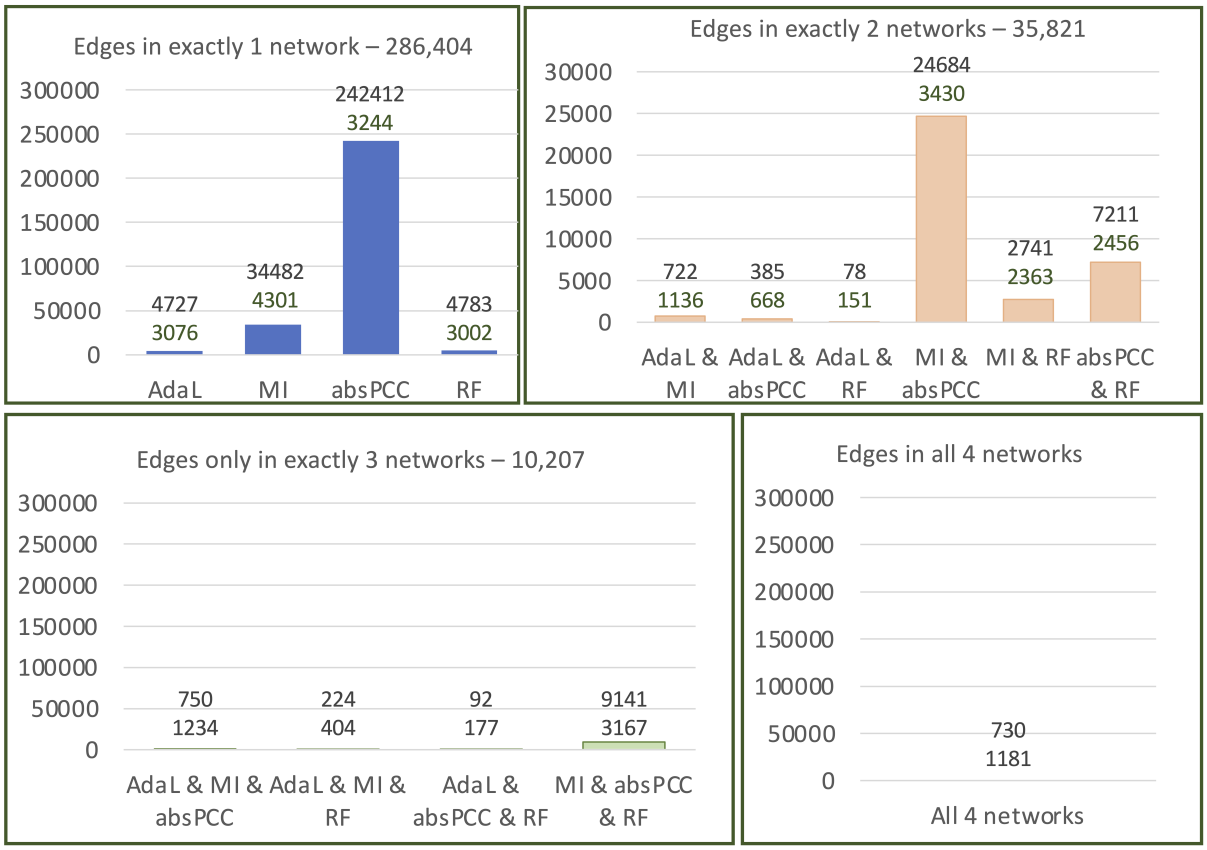

Supplementary Fig. S2. Details about pairwise edge overlap between the four networks, i.e., AdaL, MI, absPCC, RF. The box on the top left shows the number of unique edges that are only present in exactly one network, where the x-axis shows the networks and the y-axis shows the edge counts. The box on the top right shows the number of unique edges that are only present in exactly two networks, where the x-axis shows the network pairs and the y-axis shows the edge counts. The box on the left bottom shows the number of unique edges that are only present in exactly three networks, where the x-axis shows the network triplets and the y-axis shows the edge counts. The box on the right bottom shows the number of unique edges that are present in all four networks, where the x-axis shows the four networks and the y-axis shows the edge counts. The two numbers on top of each bar within each of the four boxes represent the number of edges and the number of nodes these edges encompass.

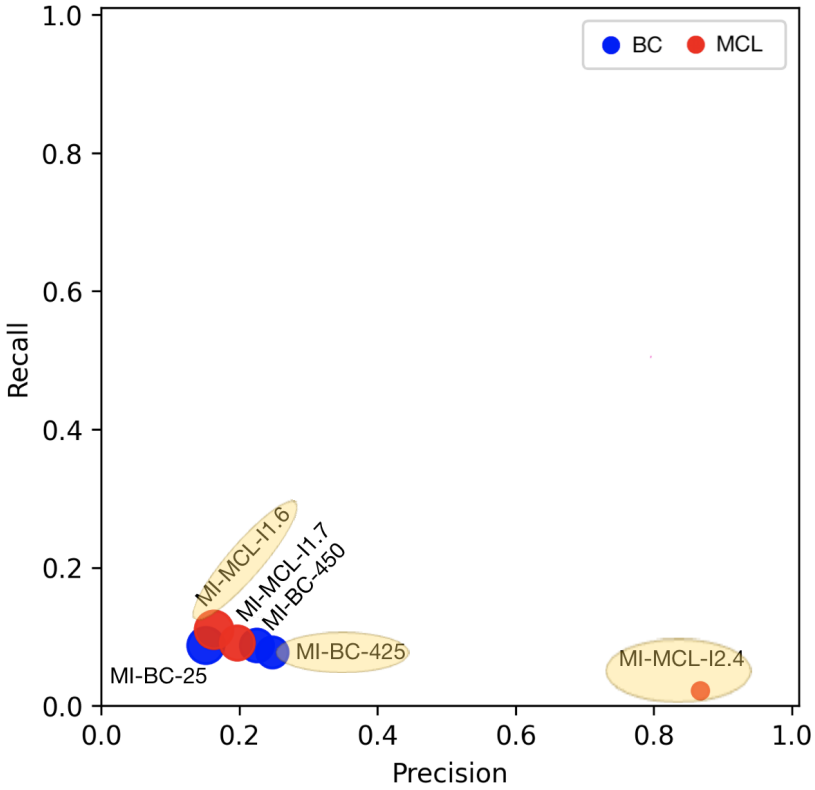

Supplementary Fig. S3. LOO prediction accuracy in terms of precision and recall for MI network. The size of each object represents the number of predictions it makes (i.e., the larger the object is, the more prediction it makes). The objects with the same shape mean they are from the same network, but have different network parameters or clustering methods (i.e., color shade).

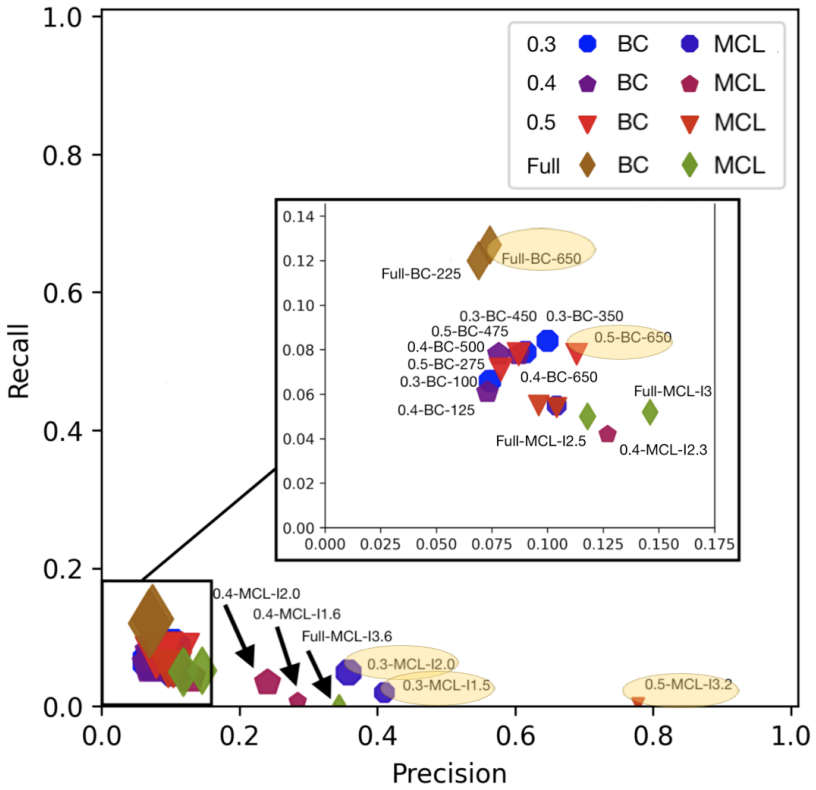

Supplementary Fig. S4. LOO prediction accuracy in terms of precision and recall for absPCC network. The size of each object represents the number of predictions it makes (i.e., the larger the object is, the more prediction it makes). The objects with the same shape mean they are from the same network, but have different network parameters or clustering methods (i.e., color shade). Note, we vary different network thresholds for the absPCC network and we present them in the same figure with different shapes.

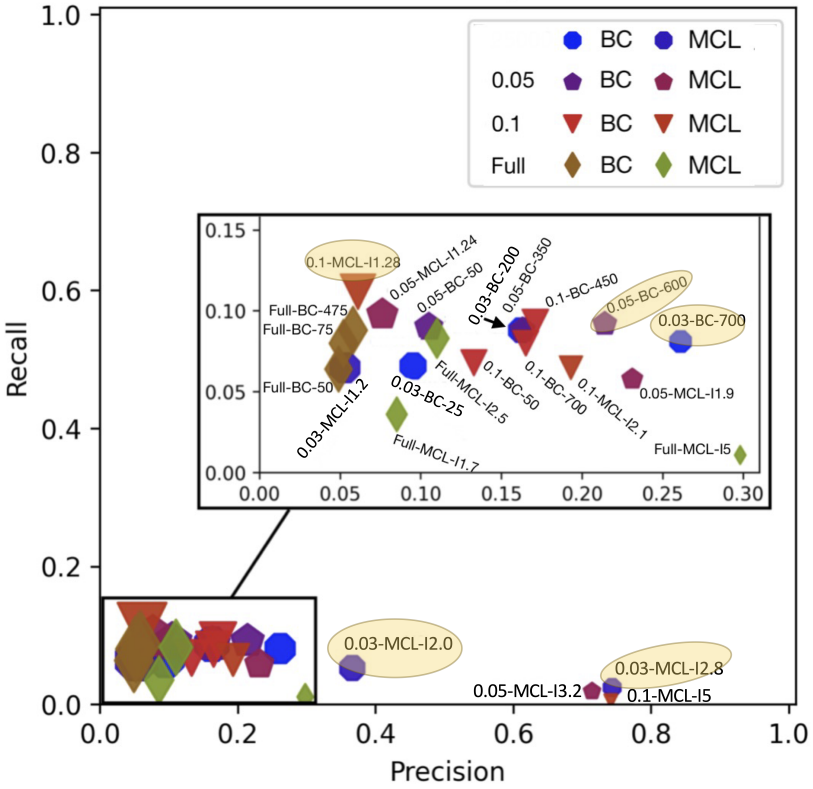

Supplementary Fig. S5. LOO prediction accuracy in terms of precision and recall for RF network. The size of each object represents the number of predictions it makes (i.e., the larger the object is, the more prediction it makes). The objects with the same shape mean they are from the same network, but have different network parameters or clustering methods (i.e., color shade). Note, we vary different network thresholds for the RF network and we present them in the same figure with different shapes.

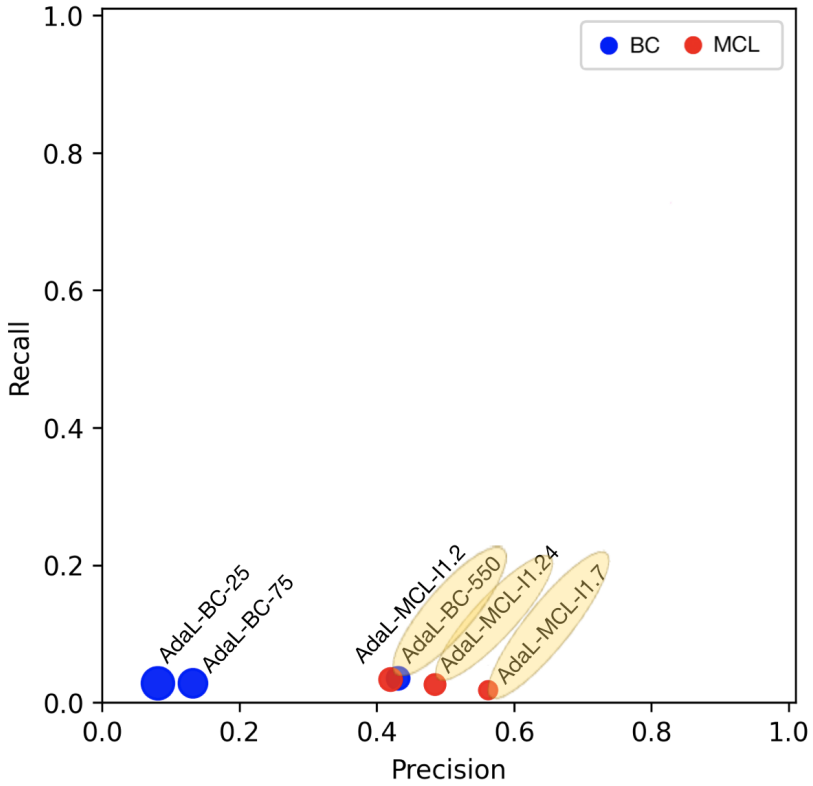

Supplementary Fig. S6. LOO prediction accuracy in terms of precision and recall for AdaL network. The size of each object represents the number of predictions it makes (i.e., the larger the object is, the more prediction it makes). The objects with the same shape mean they are from the same network, but have different network parameters or clustering methods (i.e., color shade).

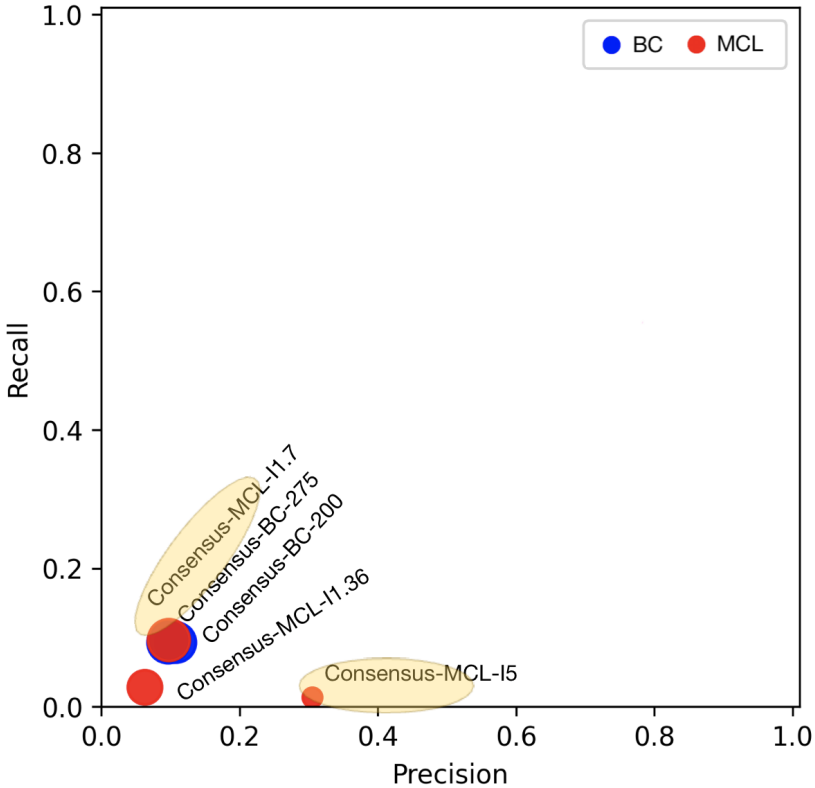

Supplementary Fig. S7. LOO prediction accuracy in terms of precision and recall for Consensus network. The size of each object represents the number of predictions it makes (i.e., the larger the object is, the more prediction it makes). The objects with the same shape mean they are from the same network, but have different network parameters or clustering methods (i.e., color shade).

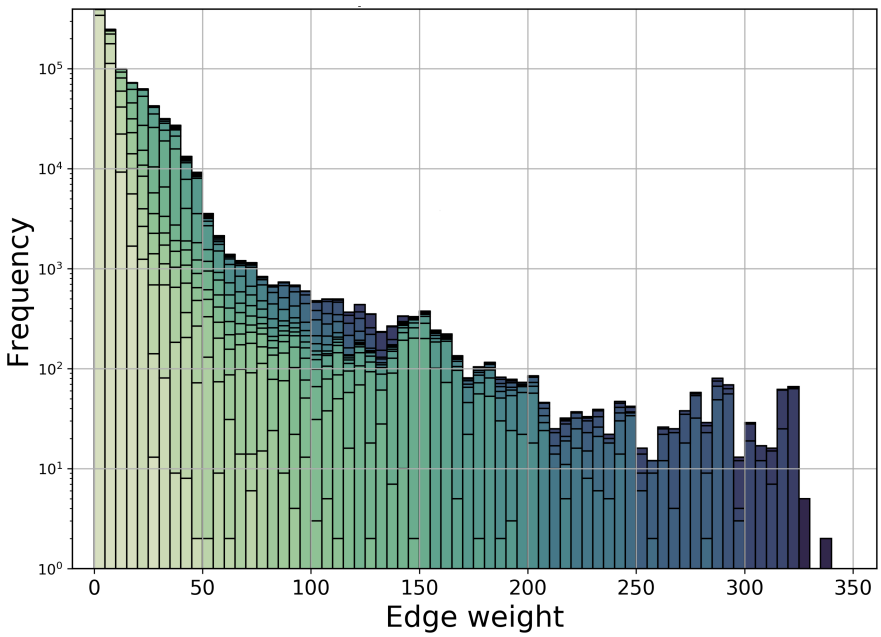

Supplementary Fig. S8. The confidence score distribution of predicted gene-gene interactions. The color shades represent the number of network_cluster combinations that support the corresponding association. The x-axis denotes edge weights of gene-gene interactions, meaning their confidence scores. The darker color is, the more network_cluster combinations support it. The caption of the x-axis describes briefly how the confidence score is calculated.

Competing interests

The authors declare that they have no competing interests.

Author's contributions

Q.L., K.B.S., M.T.F., and T.M. designed the study. Q.L. performed gene expression missing data imputation, ground truth data collection and selection, network inference, network clustering, results analysis, gene-GO term association reference list, gene-gene interaction reference list, and endocytosis validation analysis. K.B.S. performed gne expression probe-level data process, cyclical stage variation, ground truth data collection and selection, and predicted gene-GO term associations validation. Q.L. drafted the initial paper, K.B.S. contributed multiple round of writing improvement, including implementing more details, drawing workflow figure. K.M. performed initial inference of adaptive Lasso and mutual information network. M.S. performed Endocytosis data selection and biological interpretation towards results. E.C. performed Hypergeometric test validation, Endocytosis validation, and scatter plot visualization. G.F. performed Microarray probe remapping. Q.L., K.B.S., M.T.F., and T.M. contributed to the writing of the final version. All authors approved the manuscript. T.M. and M.T.F. supervised all aspects of the study.

Funding

This work is supported by NSF CAREER CCF-1452795 and National Institutes of Health grant P01 12072248 (MTF).

Acknowledgements

We thank Khalique Newaz and Shawn Gu for their comments and suggestions for the clarity of our writings.

References

1. S. H. Adjalley, D. Scanfeld, E. Kozlowski, M. Llinas, and D. A. Fidock. Genome-wide transcriptome profiling reveals functional networks involving the plasmodium falciparum drug resistance transporters pfcrt and pfmdr1. *BMC Genomics*, 16:1090, 2015.

2. M. E. Ahsen, Y. Chun, A. Grishin, G. Grishina, G. Stolovitzky, G. Pandey, and S. Bunyavanich. NeTFactor, a framework for identifying transcriptional regulators of gene expression-based biomarkers. *Scientific Reports*, 9(1):1–13, 2019.

3. M. Bansal, V. Belcastro, A. Ambesi-Impiombato, and D. Di Bernardo. How to infer gene networks from expression profiles. *Molecular Systems Biology*, 3(1):78, 2007.

4. A.-L. Barabási. Network science. *Philosophical Transactions of the Royal Society A: Mathematical, Physical and Engineering Sciences*, 371(1987):20120375, 2013.

5. A. Bauer-Mehren, M. Bundschus, M. Rautschka, M. A. Mayer, F. Sanz, and L. I. Furlong. Gene-disease network analysis reveals functional modules in mendelian, complex and environmental diseases. *PLOS ONE*, 6(6):e20284, 2011.

6. J. Benesty, J. Chen, Y. Huang, and I. Cohen. Pearson correlation coefficient. In *Noise Reduction in Speech Processing*, pages 1–4. Springer, 2009.

7. J. Birnbaum, S. Scharf, S. Schmidt, E. Jonscher, W. A. M. Hoeijmakers, S. Flemming, C. G. Toenhake, M. Schmitt, R. Sabitzki, B. Bergmann, et al. A Kelch13-defined endocytosis pathway mediates artemisinin resistance in malaria parasites. *Science*, 367(6473):51–59, 2020.

8. S. v. Buuren and K. Groothuis-Oudshoorn. MICE: Multivariate imputation by chained equations in R. *Journal of Statistical Software*, pages 1–68, 2010.

9. D. Camacho, A. De La Fuente, and P. Mendes. The origin of correlations in metabolomics data. *Metabolomics*, 1(1):53–63, 2005.

10. E. J. Candès and B. Recht. Exact matrix completion via convex optimization. *Foundations of Computational Mathematics*, 9(6):717, 2009.

11. S. B. Carey, J. Jenkins, J. T. Lovell, F. Maumus, A. Sreedasyam, A. C. Payton, S. Shu, G. P. Tiley, N. Fernandez-Pozo, A. Healey, et al. Gene-rich UV sex chromosomes harbor conserved regulators of sexual development. *Science Advances*, 7(27):eabh2488, 2021.

12. A. Dobra, C. Hans, B. Jones, J. R. Nevins, G. Yao, and M. West. Sparse graphical models for exploring gene expression data. *Journal of Multivariate Analysis*, 90(1):196–212, 2004.

13. A. M. Dondorp, F. Nosten, P. Yi, D. Das, A. P. Phyo, J. Tarning, K. M. Lwin, F. Ariey, W. Hanpithakpong, S. J. Lee, et al. Artemisinin resistance in Plasmodium falciparum malaria. *New England Journal of Medicine*, 361(5):455–467, 2009.

14. A. J. Enright, S. Van Dongen, and C. A. Ouzounis. An efficient algorithm for large-scale detection of protein families. *Nucleic Acids Research*, 30(7):1575–1584, 2002.

15. A. Gorovits, E. Gujral, E. E. Papalexakis, and P. Bogdanov. Larc: Learning activity-regularized overlapping communities across time. In *Proceedings of the 24th ACM SIGKDD International Conference on Knowledge Discovery & Data Mining*, pages 1465–1474, 2018.

16. B. Greenwood and T. Mutabingwa. Malaria in 2002, 2002.

17. F. Hahne, W. Huber, R. Gentleman, S. Falcon, S. Falcon, and R. Gentleman. Hypergeometric testing used for gene set enrichment analysis. *Bioconductor case studies*, pages 207–220, 2008.

18. A. U. Hain, A. S. Miller, J. Levitskaya, and J. Bosch. Virtual screening and experimental validation identify novel inhibitors of the Plasmodium falciparum Atg8-Atg3 protein-protein interaction. *ChemMedChem*, 11(8):900–10, 2016.

19. T. Hastie, R. Mazumder, J. D. Lee, and R. Zadeh. Matrix completion and low-rank SVD via fast alternating least squares. *The Journal of Machine Learning Research*, 16(1):3367–3402, 2015.

20. R. C. Henrici, R. L. Edwards, M. Zoltner, D. A. van Schalkwyk, M. N. Hart, F. Mohring, R. W. Moon, S. D. Nofal, A. Patel, C. Flueck, et al. The Plasmodium falciparum artemisinin susceptibility-associated AP-2 adaptin μ subunit is clathrin independent and essential for schizont maturation. *Mbio*, 11(1):e02918–19, 2020.

21. G. Hu, A. Cabrera, M. Kono, S. Mok, B. K. Chaal, S. Haase, K. Engelberg, S. Cheemadan, T. Spielmann, P. R. Preiser, et al. Transcriptional profiling of growth perturbations of the human malaria parasite Plasmodium falciparum. *Nature Biotechnology*, 28(1):91–98, 2010.

22. G. Hu, M. Llinás, J. Li, P. R. Preiser, and Z. Bozdech. Selection of long oligonucleotides for gene expression microarrays using weighted rank-sum strategy. *BMC Bioinformatics*, 8:350, 2007.

23. P. Hunt, A. Martinelli, K. Modrzynska, S. Borges, A. Creasey, L. Rodrigues, D. Beraldi, L. Loewe, R. Fawcett, S. Kumar, et al. Experimental evolution, genetic analysis and genome re-sequencing reveal the mutation conferring artemisinin resistance in an isogenic lineage of malaria parasites. *BMC Genomics*, 11(1):1–13, 2010.

24. V. A. Huynh-Thu, A. Irrthum, L. Wehenkel, and P. Geurts. Inferring regulatory networks from expression data using tree-based methods. *PLOS ONE*, 5(9):1–10, 2010.

25. M. M. Ippolito, K. A. Moser, J.-B. B. Kabuya, C. Cunningham, and J. J. Juliano. Antimalarial drug resistance and implications for the who global technical strategy. *Current Epidemiology Reports*, 8:46–62, 2021.

26. J. Iqbal, M. Al-Awadhi, and S. Ahmad. Decreasing trend of imported malaria cases but increasing influx of mixed P. falciparum and P. vivax infections in malaria-free Kuwait. *PLOS ONE*, 15(12):e0243617, 2020.

27. S. Jahagirdar, M. Suarez-Diez, and E. Saccenti. Simulation and reconstruction of metabolite–metabolite association networks using a metabolic dynamic model and correlation based algorithms. *Journal of Proteome Research*, 18(3):1099–1113, 2019.

28. K. J. Karczewski, L. C. Francioli, G. Tiao, B. B. Cummings, J. Alföldi, Q. Wang, R. L. Collins, K. M. Laricchia, A. Ganna, D. P. Birnbaum, et al. The mutational constraint spectrum quantified from variation in 141,456 humans. *Nature*, 581(7809):434–443, 2020.

29. H. Kim, G. H. Golub, and H. Park. Missing value estimation for DNA microarray gene expression data: local least squares imputation. *Bioinformatics*, 21(2):187–198, 2005.

30. D. Kochar, A. Das, A. Kochar, S. Middha, J. Acharya, G. Tanwar, D. Pakalapati, A. Subudhi, P. Boopathi, S. Garg, et al. A prospective study on adult patients of severe malaria caused by Plasmodium falciparum, Plasmodium vivax and mixed infection from Bikaner, northwest India. *Journal of Vector Borne Diseases*, 51(3):200, 2014.

31. P. Koskinen, P. Törönen, J. Nokso-Koivisto, and L. Holm. PANNZER: high-throughput functional annotation of uncharacterized proteins in an error-prone environment. *Bioinformatics*, 31(10):1544–1552, 2015.

32. N. Krämer, J. Schäfer, and A.-L. Boulesteix. Regularized estimation of large-scale gene association networks using graphical Gaussian models. *BMC Bioinformatics*, 10(1):384, 2009.

33. A. Lachmann, F. M. Giorgi, G. Lopez, and A. Califano. ARACNe-AP: gene network reverse engineering through adaptive partitioning inference of mutual information. *Bioinformatics*, 32(14):2233–2235, 2016.

34. D. J. LaCount, M. Vignali, R. Chettier, A. Phansalkar, R. Bell, J. R. Hesselberth, L. W. Schoenfeld, I. Ota, S. Sahasrabudhe, C. Kurschner, et al. A protein interaction network of the malaria parasite Plasmodium falciparum. *Nature*, 438(7064):103–107, 2005.

35. K. A. Lawson, C. M. Sousa, X. Zhang, E. Kim, R. Akthar, J. J. Caumanns, Y. Yao, N. Mikolajewicz, C. Ross, K. R. Brown, et al. Functional genomic landscape of cancer-intrinsic evasion of killing by t cells. *Nature*, 586(7827):120–126, 2020.

36. J. Le Bras and R. Durand. The mechanisms of resistance to antimalarial drugs in Plasmodium falciparum. *Fundamental & Clinical Pharmacology*, 17(2):147–153, 2003.

37. H. Li and J. Gui. Gradient directed regularization for sparse gaussian concentration graphs, with applications to inference of genetic networks. *Biostatistics*, 7(2):302–317, 2006.

38. Q. Li and T. Milenkovic. Supervised prediction of aging-related genes from a context-specific protein interaction subnetwork. *IEEE/ACM Transactions on Computational Biology and Bioinformatics*, 2021.

39. Q. Li, K. Newaz, and T. Milenković. Improved supervised prediction of aging-related genes via weighted dynamic network analysis. *BMC bioinformatics*, 22(1):1–26, 2021.

40. Q. Liao, C. Liu, X. Yuan, S. Kang, R. Miao, H. Xiao, G. Zhao, H. Luo, D. Bu, H. Zhao, et al. Large-scale prediction of long non-coding RNA functions in a coding–non-coding gene co-expression network. *Nucleic Acids Research*, 39(9):3864–3878, 2011.

41. K. Lu, K. Yang, E. Niyongabo, Z. Shu, J. Wang, K. Chang, Q. Zou, J. Jiang, C. Jia, B. Liu, et al. Integrated network analysis of symptom clusters across disease conditions. *Journal of Biomedical Informatics*, 107:103482, 2020.

42. L. Manning, M. Laman, I. Law, C. Bona, S. Aipit, D. Teine, J. Warrell, A. Rosanas-Urgell, E. Lin, B. Kiniboro, et al. Features and prognosis of severe malaria caused by Plasmodium falciparum, Plasmodium vivax and mixed Plasmodium species in Papua New Guinean children. *PLOS ONE*, 6(12):e29203, 2011.

43. D. Marbach, J. C. Costello, R. Kuffner, N. M. Vega, R. J. Prill, D. M. Camacho, K. R. Allison, R. Bonneau, Y. Chen, J. J. Collins, F. Coordero, J. C. Costello, M. Crane, F. Dondelinger, M. Drton, R. Espositoo, R. Foygel, T. D. Consortium, and G. Stolvitzky. Wisdom of crowds for robust gene network inference. *Nature Methods*, 9(8):796–804, 2012.

44. A. A. Margolin, I. Nemenman, K. Basso, C. Wiggins, G. Stolovitzky, R. Dalla Favera, and A. Califano. ARACNE: an algorithm for the reconstruction of gene regulatory networks in a mammalian cellular context. In *BMC Bioinformatics*, volume 7, pages S1–S7. Springer, 2006.

45. R. Mazumder, T. Hastie, and R. Tibshirani. Spectral regularization algorithms for learning large incomplete matrices. *The Journal of Machine Learning Research*, 11:2287–2322, 2010.

46. R. A. C. Montes, G. Coello, K. L. González-Aguilera, N. Marsch-Martínez, S. de Folter, and E. R. Alvarez-Buylla. ARACNe-based inference, using curated microarray data, of arabidopsis thaliana root transcriptional regulatory networks. *BMC Plant Biology*, 14(1):97, 2014.

47. S. Nelson-Sathi, F. L. Sousa, M. Roettger, N. Lozada-Chávez, T. Thiergart, A. Janssen, D. Bryant, G. Landan, P. Schönheit, B. Siebers, et al. Origins of major archaeal clades correspond to gene acquisitions from bacteria. *Nature*, 517(7532):77–80, 2015.

48. P. K.-S. Ng, J. Li, K. J. Jeong, S. Shao, H. Chen, Y. H. Tsang, S. Sengupta, Z. Wang, V. H. Bhavana, R. Tran, et al. Systematic functional annotation of somatic mutations in cancer. *Cancer Cell*, 33(3):450–462, 2018.

49. J. Oberstaller, T. D. Otto, J. C. Rayner, and J. H. Adams. Essential genes of the parasitic apicomplexa. *Trends in Parasitology*, 37(4):304–316, 2021.

50. J. Oliveira-Ferreira, M. V. Lacerda, P. Brasil, J. L. Ladislau, P. L. Tauil, and C. T. Daniel-Ribeiro. Malaria in Brazil: an overview. *Malaria Journal*, 9(1):1–15, 2010.

51. W. H. Organization. Malaria. *https://www.who.int/news-room/fact-sheets/detail/malaria*, 2020.

52. W. H. Organization et al. The potential impact of health service disruptions on the burden of malaria: a modelling analysis for countries in sub-Saharan Africa. *WHO*, 2020.

53. M. Pham, S. Wilson, H. Govindarajan, C.-H. Lin, and O. Lichtarge. Discovery of disease-and drug-specific pathways through community structures of a literature network. *Bioinformatics*, 36(6):1881–1888, 2020.

54. M. S. Pieperhoff, M. Schmitt, D. J. Ferguson, and M. Meissner. The role of clathrin in post-Golgi trafficking in Toxoplasma gondii. *PLOS ONE*, 8(10):e77620, 2013.

55. A. Ramaprasad, A. Pain, and T. Ravasi. Defining the protein interaction network of human malaria parasite plasmodium falciparum. *Genomics*, 99(2):69–75, 2012.

56. A. K. Rider, T. Milenković, G. H. Siwo, R. S. Pinapati, S. J. Emrich, M. T. Ferdig, and N. V. Chawla. Networks' characteristics are important for systems biology. *Network Science*, 2(2):139–161, 2014.

57. T. Rito, Z. Wang, C. M. Deane, and G. Reinert. How threshold behaviour affects the use of subgraphs for network comparison. *Bioinformatics*, 26(18):i611–i617, 2010.

58. S. S. Rund, B. Yoo, C. Alam, T. Green, M. T. Stephens, E. Zeng, G. F. George, A. D. Sheppard, G. E. Duffield, T. Milenković, et al. Genome-wide profiling of 24 hr diel rhythmicity in the water flea, Daphnia pulex: network analysis reveals rhythmic gene expression and enhances functional gene annotation. *BMC Genomics*, 17(1):653, 2016.

59. J. Schäfer and K. Strimmer. A shrinkage approach to large-scale covariance matrix estimation and implications for functional genomics. *Statistical Applications in Genetics and Molecular Biology*, 4(1), 2005.

60. G. H. Siwo, A. Tan, K. A. Button-Simons, U. Samarakoon, L. A. Checkley, R. S. Pinapati, and M. T. Ferdig. Predicting functional and regulatory divergence of a drug resistance transporter gene in the human malaria parasite. *BMC Genomics*, 16(1):1–13, 2015.

61. T. Spielmann, S. Gras, R. Sabitzki, and M. Meissner. Endocytosis in Plasmodium and Toxoplasma parasites. *Trends in Parasitology*, 36(6):520–532, 2020.

62. W. Stacklies, H. Redestig, M. Scholz, D. Walther, and J. Selbig. PCAMethods—a bioconductor package providing PCA methods for incomplete data. *Bioinformatics*, 23(9):1164–1167, 2007.

63. F. Supek, B. Matko, N. Skunca, and T. Smuc. REVIGO summarizes and visualizes long lists of Gene Ontology terms. *PLOS ONE*, 6(7):e21800, 2011.

64. D. Szklarczyk, A. L. Gable, K. C. Nastou, D. Lyon, R. Kirsch, S. Pyysalo, N. T. Doncheva, M. Legeay, T. Fang, P. Bork, et al. The STRING database in 2021: customizable protein–protein networks, and functional characterization of user-uploaded gene/measurement sets. *Nucleic Acids Research*, 49(D1):D605–D612, 2021.

65. J. Talapko, I. Škrlec, T. Alebić, M. Jukić, and A. Včev. Malaria: the past and the present. *Microorganisms*, 7(6):179, 2019.

66. Q. W. Tan and M. Mutwil. Malaria.tools—comparative genomic and transcriptomic database for Plasmodium species. *Nucleic Acids Research*, 48(D1):D768–D775, 08 2019.

67. N. Tangpukdee, C. Duangdee, P. Wilairatana, and S. Krudsood. Malaria diagnosis: a brief review. *The Korean Journal of Parasitology*, 47(2):93, 2009.

68. V. Thakur, M. Asad, S. Jain, M. E. Hossain, A. Gupta, I. Kaur, S. Rathore, S. Ali, N. J. Khan, and A. Mohmmed. Eps15 homology domain containing protein of Plasmodium falciparum (pfehd) associates with endocytosis and vesicular trafficking towards neutral lipid storage site. *Biochimica et Biophysica Acta (BBA)-Molecular Cell Research*, 1853(11):2856–2869, 2015.

69. O. Troyanskaya, M. Cantor, G. Sherlock, P. Brown, T. Hastie, R. Tibshirani, D. Botstein, and R. B. Altman. Missing value estimation methods for DNA microarrays. *Bioinformatics*, 17(6):520–525, 2001.

70. S. van Dam, U. Vosa, A. van der Graaf, L. Franke, and J. P. de Magalhaes. Gene co-expression analysis for functional classification and gene–disease predictions. *Briefings in Bioinformatics*, 19(4):575–592, 2018.

71. Y. Wang, A. Batra, H. Schulenburg, and T. Dagan. Gene sharing among plasmids and chromosomes reveals barriers for antibiotic resistance gene transfer. *Philosophical Transactions of the Royal Society B*, 377(1842):20200467, 2021.

72. Y. Wang, H. Tang, J. D. DeBarry, X. Tan, J. Li, X. Wang, T.-h. Lee, H. Jin, B. Marler, H. Guo, et al. MCScanX: a toolkit for detection and evolutionary analysis of gene synteny and collinearity. *Nucleic Acids Research*, 40(7):e49–e49, 2012.

73. M. T. Weirauch. Gene coexpression networks for the analysis of DNA microarray data. *Applied Statistics for Network Biology: Methods in Systems Biology*, 1:215–250, 2011.

74. D. J. Weiss, T. C. Lucas, M. Nguyen, A. K. Nandi, D. Bisanzio, K. E. Battle, E. Cameron, K. A. Twohig, D. A. Pfeffer, J. A. Rozier, et al. Mapping the global prevalence, incidence, and mortality of plasmodium falciparum, 2000–17: a spatial and temporal modelling study. *The Lancet*, 394(10195):322–331, 2019.

75. J. Whittaker. *Graphical Models in Applied Multivariate Statistics*. Wiley Publishing, 2009.

76. D. C. Wong, C. Sweetman, and C. M. Ford. Annotation of gene function in citrus using gene expression information and co-expression networks. *BMC Plant Biology*, 14(1):186, 2014.

77. D. Yang, Y. He, B. Wu, Y. Deng, M. Li, Q. Yang, L. Huang, Y. Cao, and Y. Liu. Drinking water and sanitation conditions are associated with the risk of malaria among children under five years old in sub-Saharan Africa: a logistic regression model analysis of national survey data. *Journal of Advanced Research*, 21:1–13, 2020.

78. J. Yang and J. Leskovec. Overlapping community detection at scale: a nonnegative matrix factorization approach. In *Proceedings of the sixth ACM International Conference on Web Search and Data Mining*, pages 587–596, 2013.

79. F.-D. Yu, S.-Y. Yang, Y.-Y. Li, and W. Hu. Co-expression network with protein–protein interaction and transcription regulation in malaria parasite plasmodium falciparum. *Gene*, 518(1):7–16, 2013. Proceedings of the 23rd International Conference on Genome Informatics (GIW 2012).